HHS Public Access

Author manuscript

Nature. Author manuscript; available in PMC 2024 July 01.

Published in final edited form as:

Nature. 2023 July ; 619(7969): 332–337. doi:10.1038/s41586-023-06246-7.

Circuit coordination of opposing neuropeptide and neurotransmitter signals

Marta E. Soden[1], **Joshua X. Yee**[1], **Larry S. Zweifel**[1,2]

[1.]Department of Pharmacology, University of Washington, Seattle WA, USA

[2.]Department of Psychiatry and Behavioral Sciences, University of Washington, Seattle WA, USA

Abstract

Fast-acting neurotransmitters and slow, modulatory neuropeptides are co-released from neurons in the central nervous system (CNS), albeit from distinct synaptic vesicles[1]. The mechanisms of how co-released neurotransmitters and neuropeptides that have opposing actions, e.g., stimulatory versus inhibitory, work together to exert control of neural circuit output remain unclear. This has been difficult to resolve due to the inability to selectively isolate these signaling pathways in a cell- and circuit-specific manner. Here, we developed a genetic-based anatomical disconnect procedure that utilizes distinct DNA recombinases to independently facilitate CRISPR/Cas9 mutagenesis[2] of neurotransmitter- and neuropeptide-related genes in distinct cell types in two different brain regions simultaneously. We demonstrate that neurons within the lateral hypothalamus (LH) that produce the stimulatory neuropeptide neurotensin (Nts) and the inhibitory neurotransmitter γ-aminobutyric acid (GABA) utilize these signals to coordinately activate dopamine neurons of the ventral tegmental area (VTA-DA). We show that GABA release from LH-Nts neurons inhibits GABA neurons within the VTA, disinhibiting dopamine neurons and causing a rapid rise in calcium, while Nts directly generates a slow inactivating calcium signal in dopamine neurons that is dependent on expression of Nts receptor 1 (Ntsr1). We further show that these two signals work together to regulate dopamine neuron responses to maximize behavioral responding. Thus, a neurotransmitter and a neuropeptide with opposing signals can act on distinct time scales through different cell types to enhance circuit output and optimize behavior.

Numerous cell types within the CNS co-release combinations of neuropeptides and neurotransmitters with opposing actions on cellular physiology[3–6]. A major unresolved question is how these opposing signals work to coordinate circuit function. An example of this paradoxical co-release is neurons in the LH that release stimulatory Nts and inhibitory GABA. The majority of Nts-producing neurons in the LH, like most LH afferents to the VTA, are reported to be GABAergic[7–9], and LH-Nts neurons are proposed to activate dopamine-producing neurons within the VTA to regulate behavioral reinforcement[9–16], but

Correspondence and requests for materials should be addressed to MES or LSZ: msoden@uw.edu, larryz@uw.edu.

Author contributions: M.E.S. and L.S.Z conceptualized the study and designed experiments. M.E.S. and J.X.Y. performed all experiments and collected data. M.E.S., J.X.Y., and L.S.Z. analyzed data and wrote the paper.

Competing Interests: The authors have no competing interests to declare.

Code availability: Code for fiber photometry analysis was derived from a publicly available source (Tucker Davis Technologies) and is available on GitHub (https://github.com/ScottNE/PEP_Distribution).

it remains unclear what the roles of Nts and GABA are in this process. We propose a circuit mechanism whereby GABA release from LH-Nts neurons inhibits local VTA-GABA neurons, which would rapidly disinhibit VTA-DA cells, while Nts acts through Ntsr1 on VTA-DA neurons to provide a slow stimulatory depolarization.

Consistent with previous reports[7,8], we found that the majority of Nts neurons in the LH are GABAergic, as evidenced by co-expression of *Nts* and *Slc32a1* (*Vgat*, the vesicular GABA transporter) (Fig. 1a–c, Supplementary Table 1). To establish the connectivity of LH-Nts neurons in the VTA, we generated double transgenic mouse lines that express Cre-recombinase from the Nts locus (*Nts*-Cre) and Flp-recombinase from the dopamine-selective tyrosine hydroxylase locus (*Th*-Flp; Extended Data Fig. 1a,b) or the Vgat locus (*Vgat*-Flp). We injected *Nts*-Cre::*Th*-Flp or *Nts*-Cre::*Vgat*-Flp mice with a Cre-conditional adeno-associated virus (AAV) containing channelrhodopsin-2[17] (AAV1-FLEX-ChR2-eYFP) into the LH and a Flp-conditional AAV encoding the fluorescent protein mCherry (AAV1-FLEXfrt-mCherry) into the VTA to mark cells for slice electrophysiology (Figure 1d). Light activation of LH-Nts inputs to the VTA generated outward inhibitory currents in VTA-GABA neurons, but we found minimal inhibitory connectivity with VTA-DA neurons (Fig. 1e–f). We detected small inward excitatory currents in fewer than 5% of VTA-GABA or VTA-DA neurons, consistent with the low expression of *Slc17a6* (*Vglut2*) in LH-Nts neurons (Fig. 1a–f).

Within the VTA, *Ntsr1* is reportedly expressed almost exclusively in DA neurons[18–20]; we confirmed this with *in situ* hybridization for *Ntsr1* and *Th* (Fig. 1g,h). Bath application of Nts evokes a depolarizing current in VTA neurons[21], and we found that this effect is selective for VTA-DA, but not VTA-GABA neurons (Fig. 1i). Consistent with the specificity of Ntsr1 in mediating the observed effects, we found that the expression of the alternate Nts receptor encoding gene, *Ntsr2*, is almost exclusively in glial cells and not neurons (Extended Data Fig. 1c–d).

We next devised a strategy that allows us to inactivate GABA release from LH-Nts neurons through Cre-dependent CRISPR/SaCas9 mutagenesis of *Vgat* and simultaneously inactivate Nts signaling in VTA-DA neurons through Flp-dependent mutagenesis of *Ntsr1*. We previously validated mutagenesis at the Vgat locus using AAV1-FLEX-SaCas9-U6-sgVgat[2]; we confirmed that this virus effectively reduces GABAergic transmission from LH-Nts to VTA-GABA neurons compared to control (AAV1-FLEX-SaCas9-U6-sgRosa26[2]; Fig. 2a). We next generated a Flp-dependent CRISPR virus containing a single guide RNA targeting *Ntsr1* (AAV-FLEXfrt-SaCas9-U6-sgNtsr1); we confirmed effective mutagenesis in *Th*-Flp neurons through DNA sequencing and nonsense mediated mRNA decay through *in situ* hybridization (Extended Data Fig. 2a–f). We also found that Nts-induced depolarization of VTA-DA neurons in slice is blocked by CRISPR/SaCas9 mutagenesis of *Ntsr1* (Fig. 2b), without affecting glutamatergic or GABAergic synaptic inputs (Extended Data Fig 2g–l).

In our proposed model (Fig. 2c and Extended Data Fig. 3a), GABA release from LH-Nts neurons onto VTA-GABA neurons disinhibits VTA-DA neurons, depolarizing these cells and activating voltage-gated calcium channels (VGCC)[22]. Activation of the Gq-coupled Ntsr1 on VTA-DA neurons by Nts release from LH-Nts neurons will also increase

intracellular calcium on a slower timescale through phospholipase C (PLC) signaling[23]. These changes in intracellular calcium can be monitored by expression of the genetically encoded calcium sensor GCaMP6m[24]. To test whether activation of LH-Nts inputs to the VTA increases intracellular calcium in dopamine neurons in a GABA- and Ntsr1-dependent manner, we expressed the red light-activated opsin Chrimson[25] in LH-Nts neurons (AAV1-FLEX-Chrimson-Tdtomato), mutated the *Vgat* locus in LH-Nts neurons alone, mutated *Ntsr1* in VTA-DA neurons alone, or mutated *Vgat* in LH-Nts neurons and *Ntsr1* in VTA-DA neurons together, while expressing GCaMP6m in VTA-DA neurons in all conditions (AAV1-FLEXfrt-GCaMP6m) (Fig. 2d; Extended Data Fig. 3b–e and Extended Data Fig. 4).

Optical stimulation of LH-Nts neurons for 1 or 3 s reliably evoked calcium signals in VTA-DA neurons during the stimulation period (Fig. 2e–f; Extended Data Fig. 5a–c). We also observed a prolonged calcium signal following stimulus offset that increased with stimulus frequency and duration (Fig. 2g; Extended Data Fig. 5d). Inactivation of *Ntsr1* in VTA-DA neurons or *Vgat* in LH-Nts neurons each reduced evoked calcium signals, but with different kinetics and frequency dependence. Targeting *Vgat* had the most pronounced effect during the stimulation period at low frequency and duration, while targeting *Ntsr1* strongly reduced the post-stimulation calcium signal, particularly at high frequencies (Fig. 2e–g; Extended Data Fig. 5a–f). Simultaneous mutagenesis of both genes in their respective cell types further reduced evoked calcium signals (Fig. 2e–g; Extended Data Fig. 5a–f).

During LH-Nts neuron stimulation at 10 Hz or higher we detected two distinct peaks in the calcium signal in VTA-DA neurons that were most prominent with the 3 s stimulation (Fig. 2e, Extended Data Fig. 5a–b). Further analysis revealed that the initial peak was reduced by inactivation of *Vgat* in LH-Nts neurons and the second peak was reduced relative to the first peak by inactivation of *Ntsr1* in VTA-DA neurons (Extended Data Fig. 5g–l). To further resolve the fast kinetics of the calcium signal, we analyzed the initial rise time during the 3 s stimulation. Mutagenesis of *Vgat* in LH-Nts neurons significantly attenuated this initial rise but *Ntsr1* mutagenesis did not affect these kinetics (Fig. 2h–i). We observed identical results when we analyzed the initial rise of the 1 s stimulation (Extended Data Fig. 6a–b). Next, we assessed the decay of the calcium signal following termination of the LH-Nts neuron stimulation. Inactivation of *Ntsr1* in VTA-DA neurons significantly increased the rate of decay (decreased *tau*) following both 1 and 3s stimulation, while inactivation of *Vgat* in LH-Nts neurons did not significantly affect decay (Fig. 2j–k and Extended Data Fig. 6c–d). These results demonstrate that GABA release from LH-Nts neurons and Ntsr1 activation regulate calcium signals in VTA-DA neurons on different time scales in a frequency-dependent manner. GABA is the primary regulator of the calcium signal at low frequencies and at the onset of high frequency stimulation, while Ntsr1 mediates a slow onset, long lasting calcium signal detectable at frequencies of 10 Hz and above, and has a larger impact than GABA on the total calcium signal at high frequencies and long durations.

We next asked how the fast transmitter and peptide components of this circuit might contribute to dopamine neuron activation during reinforcement learning. We first used photometry to record calcium signals in LH-Nts neurons while mice were trained on an operant paradigm in which one press on an active lever led to a delayed compound conditioned stimulus (CS, tone+light) followed by a food reward (Fig. 3a–b and Extended

Data Fig. 7a). We observed a small decrease in fluorescence during the CS presentation on day 1, and a large increase in fluorescence upon head entry into the food hopper to retrieve the reward on both day 1 and day 5 of training (Fig. 3d), consistent with a proposed role for LH-Nts neurons in feeding behavior[26].

Next we recorded calcium signals in dopamine neurons following CRISPR targeting of *Vgat* in LH-Nts neurons, *Ntsr1* in VTA-DA neurons, or both, while mice were trained on the same operant paradigm (Fig. 3e and Extended Data Fig. 7b). We observed large calcium signals time-locked to reward retrieval head entries in VTA-DA neurons on day 1 of training (Figure 3f). Combined CRISPR targeting of *Vgat* and *Ntsr1* reduced the peak of this calcium signal, reduced the AUC during the prolonged decay of the signal following the head entry, and increased the rate of decay compared to control (Fig. 3g–i). Control and sgVgat animals showed a smaller head entry response on day 5 of training compared to day 1 (Fig. 3j–k and Extended Data Fig.8a–d), consistent with models of reward prediction error[27]. The AUC during the post-head entry period remained reduced in sgVgat+sgNtsr1 mice on day 5 (Fig. 3l), and the rate of decay was significantly faster in sgNtsr1 alone and sgVgat+sgNtsr1 animals compared to control (Fig. 3m), consistent with Ntsr1 mediating the slow calcium signal.

Calcium signals in dopamine neurons in response to the lever press and cue were not different between groups (Extended data Fig. 8e–l), and we did not observe a significant difference in the total number of earned reinforcers (Extended data Fig. 8m–q). As mice become proficient at acquiring reinforcers, they begin to show signs of satiety. Consistent with this phenomenon, on the last day of conditioning we found that the mean latency to retrieve the food pellet was significantly slower in the final quarter of the session compared to the first quarter, an effect not seen on the first day of conditioning when mice are just learning the task (Extended data Fig. 8r–s). Mice with combined mutagenesis of Vgat and Ntsr1 had significantly longer latencies in the last quartile compared to controls, indicating a potential role for these combined signals in regulating satiety. Intriguingly, in a separate cohort of mice we observed that sgVgat+sgNtsr1 mice exhibit a significant loss of body weight compared to controls 5 weeks post-viral injection (Extended data Fig. 8t). Similar results were found after silencing LH-Nts neurons with Cre-dependent expression of the tetanus toxin light chain (AAV1-FLEX-GFP-TeTox; Extended data Fig. 8t), indicating an important role for Nts and GABA signaling in this circuit for body weight regulation.

Activation of LH-GABA inputs to the VTA is reinforcing[9,15], and our observations that GABA release from LH-Nts neurons and Ntsr1 signaling in dopamine neurons work together to regulate calcium dynamics in VTA dopamine neurons during reward retrieval is consistent with a role for these signals in mediating the reinforcing effects of food. However, these findings do not directly demonstrate the coordinate activity of these signals at the level of LH-Nts terminals within the VTA. To determine whether activation of LH-Nts terminals in the VTA is sufficient to promote behavioral reinforcement in a manner that is dependent on both Nts and GABA, we inactivated *Ntsr1* in VTA-DA neurons or *Vgat* in LH-Nts neurons as above, expressed Chrimson-tdTomato in LH-Nts neurons, and stimulated the axon terminals of these cells within the VTA during a real-time place preference assay (Fig. 4a). Stimulation of LH-Nts inputs (20 Hz) promoted a preference for the light-paired

chamber and neither inactivation of *Ntsr1* nor *Vgat* affected this preference (Fig. 4b; Extended Data Fig. 9a–b); however, inactivation of both genes simultaneously blocked this behavioral response (Fig. 4a; Extended Data Fig. 9a–b).

To better resolve the interaction between Ntsr1 signaling in VTA-DA neurons and GABA release from LH-Nts neurons, as well as the frequency dependence of this interaction, we trained mice on a fixed-ratio schedule 1 (FR1) operant (lever press) reinforcement task for optical activation of LH-Nts terminals in the VTA. Activation of LH-Nts inputs to the VTA (40 Hz, 3 s) resulted in robust lever pressing in control mice (Fig. 4c; Extended data Fig. 9c). Mice with inactivation of *Vgat* in LH-Nts neurons or *Ntsr1* in VTA-DA neurons both learned to lever press at this stimulation frequency (Fig. 4c; Extended Data Fig. 9d–e); however, inactivation of *Ntsr1* significantly reduced lever pressing relative to controls (Fig. 4c). Mutagenesis of both *Ntsr1* in VTA-DA neurons and *Vgat* in LH-Nts neurons prevented the acquisition of this response (Fig. 4c; Extended Data Fig. 9f). Following FR1 training for 40 Hz stimulation, we assayed mice in a frequency-response assay. Mice were allowed to lever press for optical activation of LH-Nts inputs at 5, 10, 20, or 40 Hz. Control mice displayed a robust frequency-response curve for activation of LH-Nts inputs to the VTA (Fig. 4d; Extended Data Fig. 9g) that was significantly attenuated following inactivation of either *Vgat* or *Ntsr1* (Fig. 4d; Extended Data Fig. 9h–i) and was completely blocked by mutagenesis of both genes in their respective cell types (Fig. 4d; Extended Data Fig. 9j).

Our results demonstrate that GABA release from LH-Nts neurons and Ntsr1 activation in VTA-DA neurons are both required for optimal behavioral reinforcement following activation of LH-Nts terminals in the VTA but do not directly demonstrate that Nts and GABA co-release from LH-Nts neurons mediates this effect. To address this, we inactivated the *Nts* gene (AAV1-FLEX-SaCas9-U6-sgNts; Extended Data Fig. 10a–d) or both *Nts* and *Vgat* in LH-Nts neurons and repeated the experiments described above. Like mutagenesis of *Ntsr1* in VTA-DA neurons, inactivation of *Nts* did not affect RTPP, but inactivation of both *Nts* and *Vgat* did prevent this preference (Fig. 4e–f; Extended Data Fig. 10e–f). Like inactivation of *Ntsr1*, mutagenesis of *Nts* significantly attenuated the acquisition of operant stimulation of LH-Nts terminals in the VTA and the frequency-response profile, which was further reduced by inactivation of both *Vgat* and *Nts* (Fig. 4g–h; Extended Data Fig. 10g–l).

These results provide a mechanism for how Nts and GABA co-released from LH-Nts neurons contribute to behavioral reinforcement through projections to the VTA, and show how co-release of a neurotransmitter and neuropeptide with ostensibly opposing effects on cell physiology (depolarization versus hyperpolarization) can work coordinately to promote activation of a circuit node by acting at different time scales on distinct cell types (see Supplementary Material for additional discussion). These findings also provide new insights into the circuit organization of the mesolimbic dopamine system. Given the large number of GABAergic inputs to the VTA that disinhibit dopamine neurons and are likely to co-release excitatory peptides[9,28], as well as the enrichment of many peptide receptors on dopamine neurons[29], the results shown here may reflect a common mechanism for regulation of the dopamine system. Our experimental approach for *in vivo* isolation and manipulation of distinct signaling components within cells and circuits can be easily adapted going forward

to investigate other peptidergic inputs to the VTA, as well as peptidergic circuits throughout the brain to address these fundamental questions.

Methods

Mice:

All procedures were approved and conducted in accordance with the guidelines of the Institutional Animal Care and Use Committee of the University of Washington. Mice were group-housed on a 12-hour light/dark cycle with ad libitum food and water. Approximately equal numbers of male and female mice were used for all experiments. Nts-Cre mice (Jax Stock Number 017525) and Vgat-Flp mice (Jax Stock Number 029591) are available from Jackson Labs. Th-Flp mice[30] were a generous gift from Dr. Rajeshwar Awatramani.

Viruses:

All AAV1 viruses were produced in-house with titers of 1-3 $x10^{12}$ particles per mL as described[31].

Surgery:

Mice were anesthetized with isoflurane before and during viral injection and fiber implantation. Mice recovered for at least 4 weeks prior to experimentation. For slice electrophysiology, mice were injected at approximately 5-6 weeks of age. For all other experiments, mice were injected at 8-12 weeks of age. LH coordinates were M-L: 1.0, A-P: −1.25, D-V: −5.0. VTA coordinates were M-L: 0.5, A-P: −3.25, D-V:−4.25. Values are in mm, relative to bregma. A-P values were adjusted for bregma-lambda distance using a correction factor of 4.21 mm. For Z values the syringe was lowered 0.5 mm past the indicated depth and raised up at the start of the injection. Injection volume was 500 nl. Injections for slice electrophysiology and behavioral photometry were bilateral; injections for stimulated photometry and optogenetic behavior were unilateral.

Fiber optic cannulas for *in vivo* Chrimson stimulation were manufactured in-house using 1.25 mm ceramic ferrules (Kientec) and 200 μm 0.22 NA fiber (ThorLabs). Fiber optic cannulas for photometry (400 μm fiber, 0.66 NA, 1.25 mm ferrule) were from Doric. For photometry, the imaging cannula was implanted in the VTA at a depth of −4.2 mm from bregma. The stimulating cannula was implanted above the ipsilateral LH at a depth of −4.8 mm and an angle of 5°. For optogenetic behavior experiments, a stimulating cannula was implanted above the VTA at a depth of −4.0 mm from Bregma.

In Situ Hybridization:

RNAscope (Advanced Cell Diagnostics) *in situ* hybridization was performed according to manufacturer's instructions on 20 μm fresh-frozen coronal brain sections. Version 1 was used to probe for *Nts*, *Cre, Slc32a1*, and *Slc17a6* in the LH, and *Th* and *Flp* in the VTA. Version 2 was used to probe for *Ntsr1*, *Ntsr2*, *Th*, and *Gfap* in the VTA. 20x images were collected using a Leica SP8X confocal microscope and were analyzed using ImageJ software. For quantification of mRNA reduction by sgNts, mice were injected in one hemisphere with sgRosa26 and in the other hemisphere with sgNts. The integrated

pixel intensity of all Nts positive neurons in the LH was summed for each hemisection and compared to the opposite hemisection. For quantification of mRNA reduction by sgNtsr1 separate mice were injected with either sgRosa or sgNtsr1, to avoid potential spread across the midline. The integrated pixel intensity of the *Ntsr1* signal was calculated across the entire VTA for each section and compared across mice.

Slice Electrophysiology:

Horizontal brain slices (200 μm) were prepared in an ice slush solution containing (in mM): 92 NMDG, 2.5 KCl, 1.25 NaH_2PO_4, 30 $NaHCO_3$, 20 HEPES, 25 glucose, 2 thiourea, 5 Na-ascorbate, 3 Na-pyruvate, 0.5 $CaCl_2$, 10 $MgSO_4$, pH 7.3-7.4[32]. Slices recovered for ≤12 min in the same solution at 32°C and then were transferred to a room temperature solution including (in mM): 92 NaCl, 2.5 KCl, 1.25 NaH_2PO_4, 30 $NaHCO_3$, 20 HEPES, 25 glucose, 2 thiourea, 5 Na-ascorbate, 3 Na-pyruvate, 2 $CaCl_2$, 2 $MgSO_4$. Slices recovered for an additional 45 min before recordings were made in ACSF at 32°C continually perfused over slices at a rate of ~2 ml/min and containing (in mM): 126 NaCl, 2.5 KCl, 1.2 NaH_2PO_4, 1.2 $MgCl_2$ 11 D-glucose, 18 $NaHCO_3$, 2.4 $CaCl_2$. All solutions were continually bubbled with O_2/CO_2. Whole-cell recordings were made using an Axopatch 700B amplifier (Molecular Devices) with filtering at 1 kHz using 4-6 MΩ electrodes. For light-evoked PSC and bath Nts recordings electrodes were filled with an internal solution containing (in mM): 130 K-gluconate, 10 HEPES, 5 NaCl, 1 EGTA, 5 Mg-ATP, 0.5 Na-GTP, pH 7.3, 280 mOsm. Light-evoked synaptic transmission was induced with 5 ms light pulses delivered at 0.1 Hz from an optic fiber placed directly in the bath. Light-evoked EPSCs were measured with holding at −70 mV and light-evoked IPSCs were measured with holding at −30 mV. Amplitudes were calculated from an average of at least 10 events. Cells with a detectable event of at least 10 pA were counted as connected. For bath application of NTS, cells were held at −60 mV and NTS (Sigma) was washed on for 2 min. The 1000 nM Th+ group in Fig 1i is the same as the control group in Fig. 2b. Spontaneous EPSCs were recorded using the K-gluconate internal solution described above with holding at −60 mV in the presence of picrotoxin (100 μM). Spontaneous IPSCs were recorded with an internal solution containing (in mM): 135 KCl, 12 NaCl, 0.5 EGTA, 10 HEPES, 2.5 Mg-ATP, 0.25 Na-GTP, pH 7.3, 280 mOsm. sIPSC recordings were made with holding at −60 mV in the presence of kynurenic acid (2 mM). Events were analyzed using Clampfit software (Molecular Devices).

Design of CRISPR constructs:

Single guide RNAs targeting *Ntsr1* and *Nts* were designed as described[33]. Primers used for cloning sgNtsr1 into AAV1-FLEXfrt-SaCas9-U6 were: forward CACCGCATCGTCTCCAGTCCGAACT and reverse AAACAGTTCGGACTGGAGACGATGC. Primers used for cloning sgNts into AAV1-FLEX-SaCas9-U6 were: forward CACCGACGTTATCAAGGATATCTTC and reverse AAACGAAGATATCCTTGATAACGTC. AAV1-FLEX-SaCas9-U6-sgVgat and AAV1-FLEX-SaCas9-U6-sgRosa26 were previously published[2]. For all CRISPR experiments, control mice were injected with AAV1-FLEX-SaCas9-U6-sgRosa26 (LH) or AAV1-FLEXfrt-SaCas9-U6-sgRosa26 (VTA)[2].

Validation of mutagenesis:

Validation of mutagenesis was performed using fluorescence activated cell sorting (FACS), whole-genome amplification (WGA), and sequencing as described[2]. Briefly, 3 Th-Flp mice were injected in the VTA with AAV1-FLEXfrt-SaCas9-U6-sgNtsr1 along with AAV-FLEXfrt-EGFP-KASH to label nuclei for sorting. Four weeks following injection tissue punches of the VTA were collected and EGFP-positive nuclei were isolated using FACS. WGA (REPLI-g, Qiagen) was performed according to manufacturer's instructions followed by targeted sequencing of a 200-300 bp region surrounding the intended cut site. Tracking of indels by decomposition (TIDE) analysis[34] was performed to compare sequence chromatograms from EGFP negative and EGFP positive samples to estimate mutation frequency.

Fiber photometry:

Mice were connected to stimulating and imaging patch cords or the imaging patch cord alone (Doric Lenses) and placed into an operant chamber. The imaging patch cord was photobleached prior to recording. Recordings were made using an RZ5 BioAmp Processor and Synapse software (Tucker Davis Technologies). A 465 nm LED (531-Hz, sinusoidal, Doric Lenses) was used to excite GCaMP6m. LED intensity was measured at the tip of the optic fiber prior to each recording session and set to 30-40 μW. GCaMP6m fluorescence (525 ± 25 nm) was returned through the same patch cord, bandpass filtered, and recorded by the RZ5. A 405 nm LED (211-Hz, sinusoidal) was used to monitor the isosbestic signal. The 531-Hz and 211-Hz signals were extracted by Synapse software at a sampling rate of 1017.25 Hz. For stimulation experiments, red light (640 nm, 5 mW, 5 ms pulses) was delivered through the stimulating patch cord via a laser (LaserGlow) driven by the RZ5. Mice received 5 presentations of each stimulus frequency (5, 10, 20, and 40 Hz) at each duration (1 and 3 s). Stimuli were presented once per minute in a pseudo-random order. Stimulus onsets, lever press, cue, and head entry events were synced to the photometry recording via TTL delivery for offline analysis. A custom Python script derived from the epoch averaging code provided by Tucker Davis was used to extract and analyze the GCaMP signal surrounding each event. A 30 s window was extracted surrounding each red light stimulus and rewarded lever press (10 s prior and 20 s following), and a 40 s window was extracted surrounding the first head entry following reward delivery (20 s prior and 20 s following). The first 4 s of this window was used as a baseline to calculate the Z-score. For stimulation events, Z-scores for the 5 presentations of each stimulus were averaged for each mouse. For behavioral events, Z-scores for the first 20 events in the session were averaged for each mouse.

For stimulation experiments area under the curve during the 1 or 3 s stimulus and 10 s following stimulus termination was calculated relative to the 1 s period prior to stimulation. Peak amplitudes were measured as the maximum value in a 100 ms window surrounding the time of the average initial and final peak measured at 40 Hz in control mice. To quantify the initial rise, a linear regression was performed on the first 20 ms following the stimulus onset. The decay time constant (Tau) was calculated as the time for the signal to decay to 1/e of the final peak amplitude. Maximum values for Tau were capped at 8 s for stimulated photometry and 30 s for behavioral photometry. Note: For Fig.2k analysis of 5 Hz was omitted due to

lack of signal in sgVgat mice, and sgVgat+sgNtsr1 mice were excluded from analysis due to the low amplitude of the evoked fluorescence.

Delayed cue operant task:

Mice were food restricted to 85% of ad libitum body weight. Mice received one 30-minute session of acclimation to the photometry patch cord (Doric Lenses) in the operant chamber (MedAssociates), followed by two pre-training days. On pre-training day 1 mice received 20 non-contingent pellets dispensed with a variable 90 s ITI. On pre-training day 2 the house light was illuminated and both levers were extended. A press on either lever led to extinction of the house light and immediate pellet delivery, followed by a 3 sec ITI. Mice were allowed a maximum of 20 pellets. Next, mice experienced 5 days of delayed cue training, in which both levers were extended but only one lever was active. A press on the active lever led to a 3 s delay, followed by a delivery of a 3 s compound cue (lever light plus 4 KHz tone), followed by pellet delivery. The house light extinguished after each rewarded press and came back on after a 12.5 s ITI to signal the start of a new trial. Training sessions lasted for 1 hour.

Optogenetics:

Real-time place preference: On day 1, mice were connected to a patch cable and placed into a two-chambered arena and allowed to explore freely for 10 min. Mice were then assigned a light-paired chamber such that any inherent side bias was cancelled out within groups. On day 2, mice were connected to a patch cable and placed into the unpaired chamber to begin the trial. 20 Hz, 5 ms red light stimulation (1 mW) was delivered whenever the center point of the mouse was in the paired chamber (controlled by Ethovision software, Noldus). The trial lasted for 20 min.

Intracranial self-stimulation: Mice were food restricted to 85% of ad libitum body weight to increase exploratory activity. Mice were connected to a patch cable and placed into an operant chamber (MedAssociates) for a 1-hour session each day for 4 days. Each session began with a 5 min “magazine” period in which both levers extended for 10 s, followed by lever retraction and delivery of a 3 s red laser light stimulation at 40 Hz (5 ms pulse duration, 5 mW). A press on the active lever during this 10 s period resulted in immediate lever retraction and red-light delivery. Mice received 10 magazine trials with a variable 30 s ITI. For the remainder of the session, levers extended and remained extended until a press was made on the active lever, which led to lever retraction and 3 s of 40 Hz light stimulation. Levers re-extended following an additional 2 s timeout period.

Following 4 days of training at 40 Hz, mice were tested once per day in a 30-min session with the stimulus frequency set to 5, 10, 20, or 40 Hz (one frequency per day, presented in a randomized order). Frequency testing sessions began with a 3-min magazine period with stimulation at the relevant frequency.

Immunohistochemistry:

Mice were perfused with 4% PFA. For confirmation of viral expression and fiber placements 50 μm frozen brain sections were collected and stained overnight. To quantify viral co-expression 30 μm frozen brain sections were collected and stained overnight. Antibodies

used were Rabbit anti-HA (Sigma H6908, 1:1000), Chicken anti-GFP (AbCam 13970, 1:8000), and Mouse anti-DSRed (Clontech 632392, 1:2000). Secondary antibodies were from Jackson ImmunoResearch (1:250 dilution). Images were collected using a Keyence BZ-X710 fluorescent microscope and analyzed using ImageJ software.

Statistics and Reproducibility:

All data were analyzed for statistical significance using Prism software (GraphPad Prism 9). See Supplementary Table 2 for details on all statistical tests performed. The Geisser-Greenhouse correction was used to correct for unequal variability of differences in repeated-measures ANOVA tests. No statistical methods were used to predetermine sample sizes. All behavioral assays were repeated in a minimum of two cohorts with similar replication of results. Littermates were randomly assigned to experimental groups and mice were tested in random order. Mice with missed viral injections or significant viral spread outside the targeted region were excluded from analyses. Data were analyzed by an investigator blinded to experimental condition; the experimenter was not blinded during data collection

Extended Data

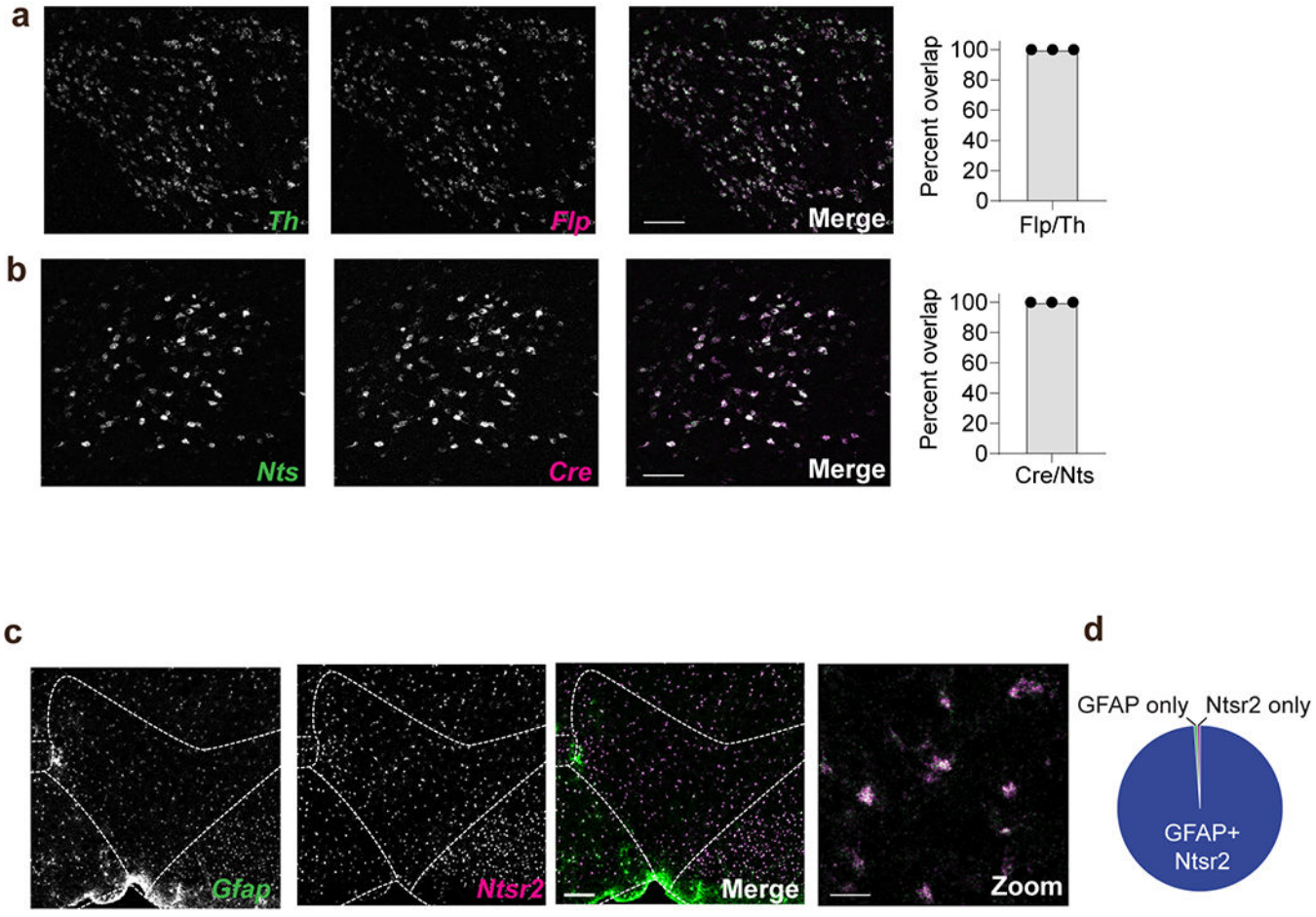

Extended Data Fig. 1. Confirmation of specific recombinase expression and analysis of *Ntsr2* expression.

(a) Example images of *in situ* hybridization for *Th* and *Flp* recombinase in the VTA of Nts-Cre::Th-Flp mice, and percentage of *Flp*+ cells that expressed *Th* (n=9 sections from N=3 mice, 4332 total *Flp*+ cells, scale bar=100 μm). **(b)** Example images of *in situ* hybridization for *Nts* and *Cre* in the LH of Nts-Cre::Th-Flp mice, and percentage of *Cre*+ cells that expressed *Nts* (n=7 sections from N=3 mice, 1058 total *Cre*+ cells). **(c)** *In situ* hybridization for the astrocyte marker *Gfap* and *Ntsr2* in the VTA. Scale bars = 150 μm (greyscale images) and 25 μm (zoom). (**d**) Quantification of *Ntsr2* and *Gfap* overlap in the VTA (n=6 sections from N=2 mice). See Supplementary Table 1 for cell counts.

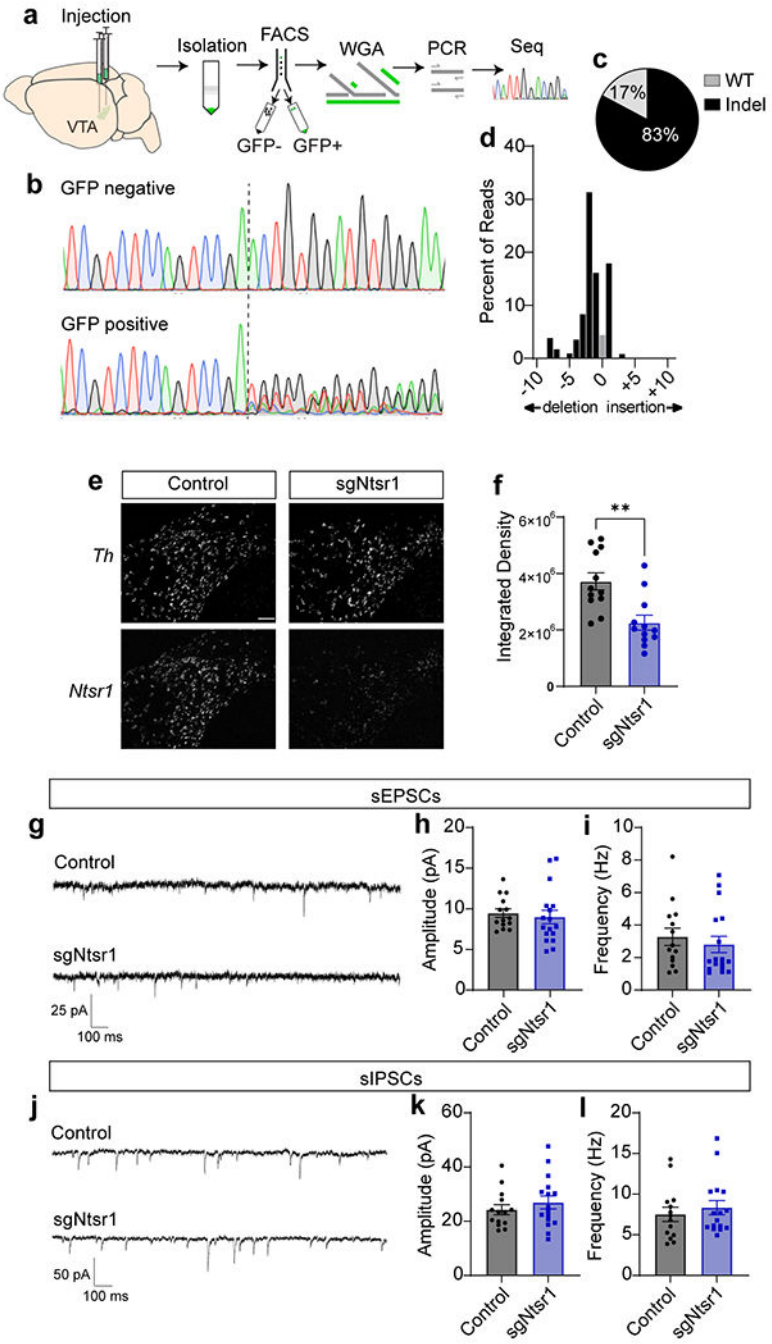

Extended Data Fig. 2. Validation of AAV1-FLEXfrt-SaCas9-U6-sgNtsr1.

(a) Schematic of procedure for isolating GFP positive nuclei infected with sgNtsr1 CRISPR virus and nuclear envelope marker KASH-GFP followed by targeted sequencing of the intended cut site. **(b)** Sanger sequencing of pooled GFP negative and positive nuclei showing a disruption in the sequence at the intended cut site (dashed line) in GFP positive nuclei only. **(c)** Estimated percentage of WT and mutated (Indel) reads in GFP positive nuclei based on TIDE analysis. **(d)** Estimated percentage of each insertion and deletion mutation based on TIDE analysis. (**e**) Example *in situ* images and (**f**) quantification of integrated

pixel density of the *Ntsr1* mRNA fluorescent signal in the VTA in mice expressing a control CRISPR or sgNtsr1. (Scale bar=100 μm. n=12 sections from N=4 mice for each group. **P<0.01.) **(g)** Example traces of spontaneous EPSCs recorded from VTA DA neurons expressing a control CRISPR or sgNtsr1. **(h-i)** sEPSC amplitude (**h**) and frequency (**i**) (control n=14 cells from N=2 mice, sgNtsr1 n=17 cells from N=2 mice). **(j)** Example traces of spontaneous IPSCs recorded from VTA DA neurons expressing a control CRISPR or sgNtsr1. **(k-l)** sIPSC amplitude (**k**) and frequency (**l**) (control n=14 cells from N=2 mice, sgNtsr1 n=16 cells from N=2 mice). Data are presented as mean ± S.E.M.

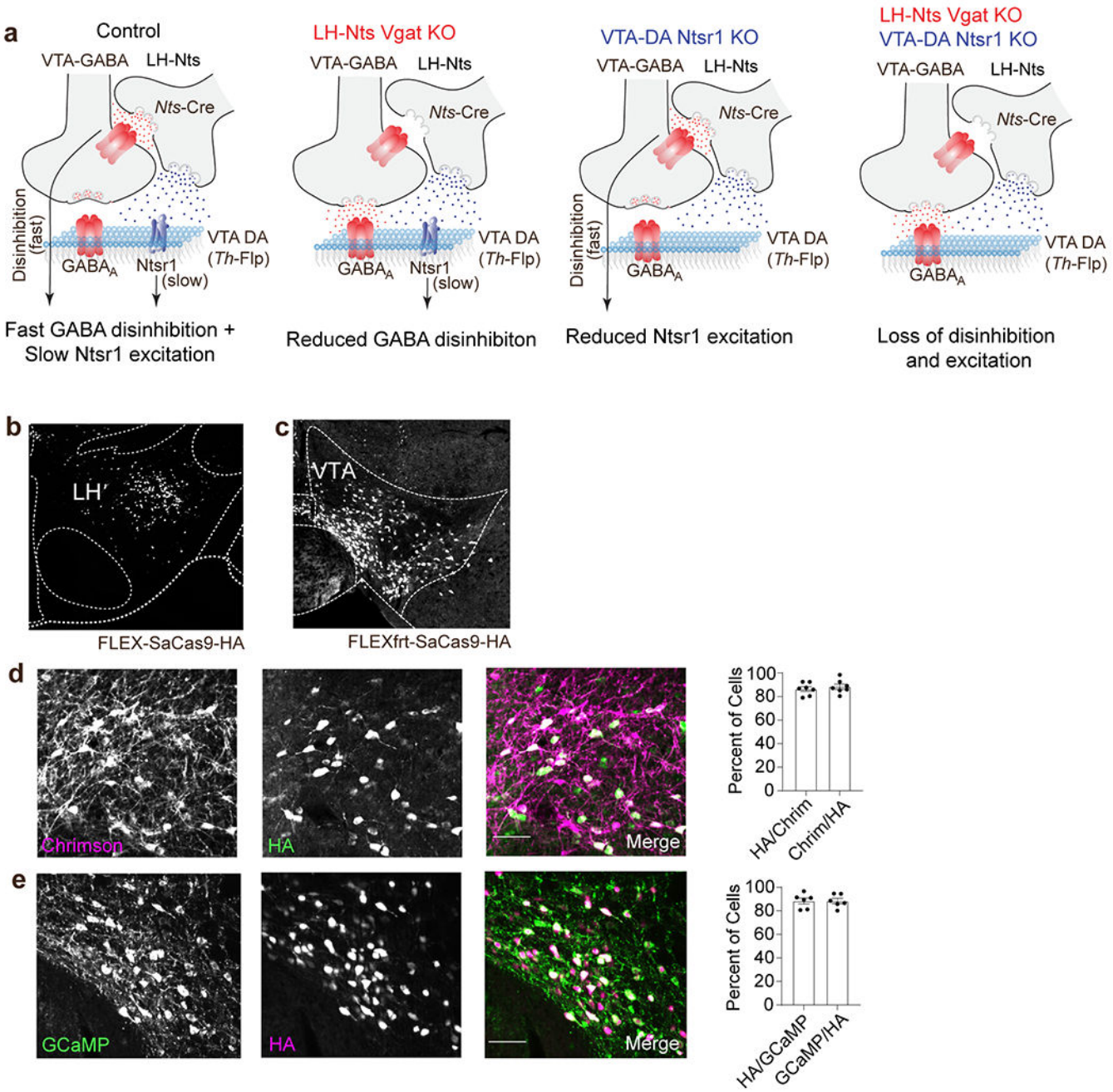

Extended Data Fig. 3: Genetic strategy for anatomical disconnect and validation of viral co-expression.

(**a**) Cartoon illustrating hypothetical co-release of GABA and Nts from LH-Nts inputs to the VTA (Note: the axo-axonic connection is presented for simplicity and is not meant to reflect the only type of synapse involved in co-release). Inactivation of Vgat from LH-Nts neurons (LH-Nts GABA KO) is predicted to blunt disinhibition. Inactivation of Ntsr1 (VTA-DA Ntsr1 KO) is predicted to prevent Nts signaling onto VTA-DA neurons and blunt slow depolarization. Loss of both Vgat and Ntsr1 (LH-Nts GABA KO + VTA-DA Ntsr1 KO) is predicted to blunt both fast and slow depolarization of the VTA-DA neurons following activation of LH-Nts inputs. **(b)** Cre-dependent expression of SaCas9 in LH-Nts neurons from AAV1-FLEX-SaCas9-U6-sgVgat detected by immunostaining for HA tag. (**c**) Flp-dependent expression of SaCas9 in VTA-DA neurons from AAV1-FLEXfrt-SaCas9-U6-sgNtsr1 detected by immunostaining for HA tag. **(d)** Example images and quantification of co-expression of AAV1-FLEX-Chrimson-tdTomato and AAV1-FLEX-SaCas9-U6-sgVgat in the LH of Nts-Cre mice (n=7 sections from N=6 mice). **(e)** Example images and quantification of co-expression of AAV1-FLEXfrt-GCaMP6m and AAV1-FLEXfrt-SaCas9-U6-sgNtsr1 in the VTA of Th-Flp mice (n=6 sections from N=3 mice). Data are presented as mean ± S.E.M.

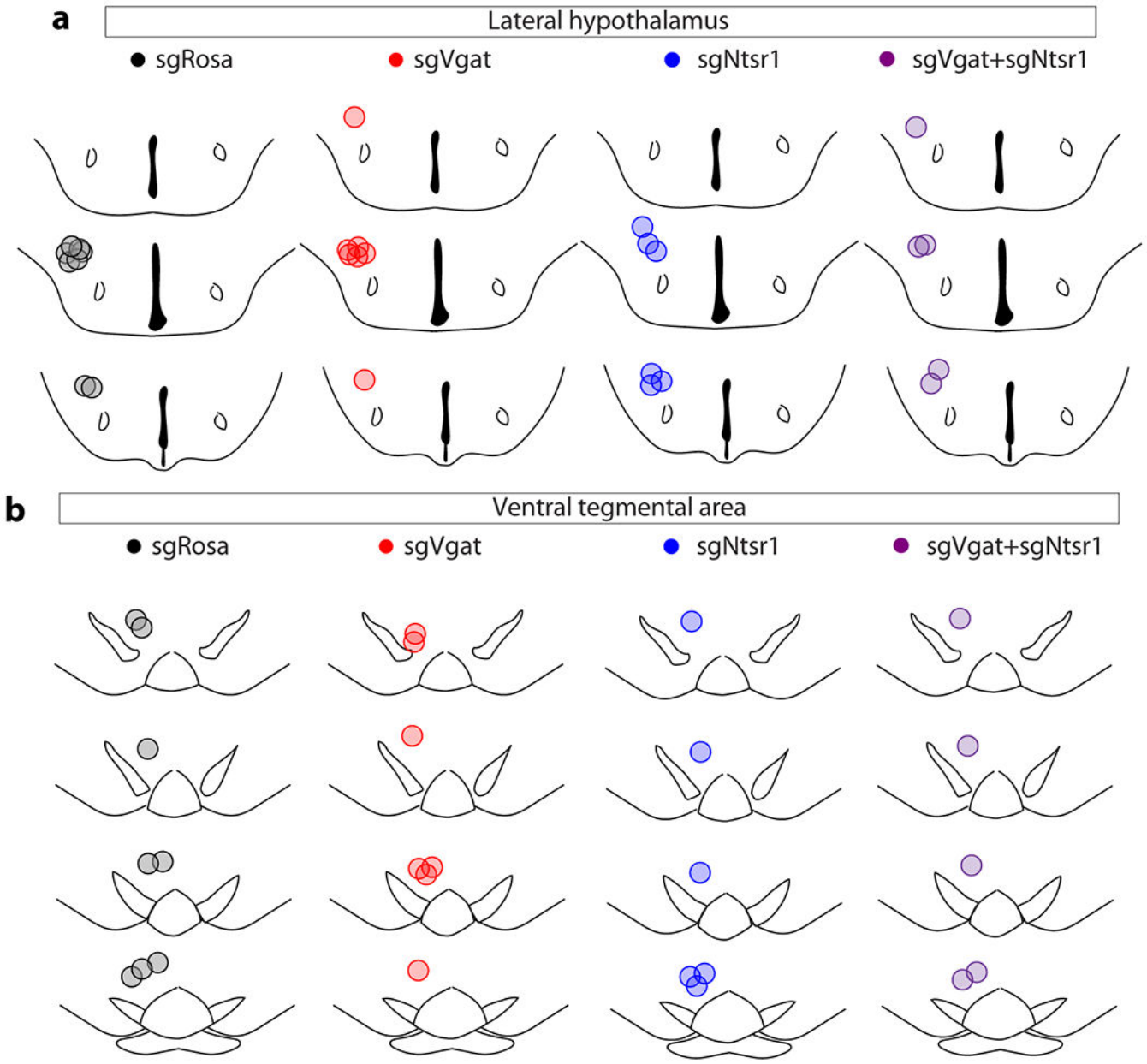

Extended Data Fig. 4: Fiber placements for stimulation photometry experiments.
(a) Placements for stimulatory fibers in LH. **(b)** Placements for recording fibers in VTA.

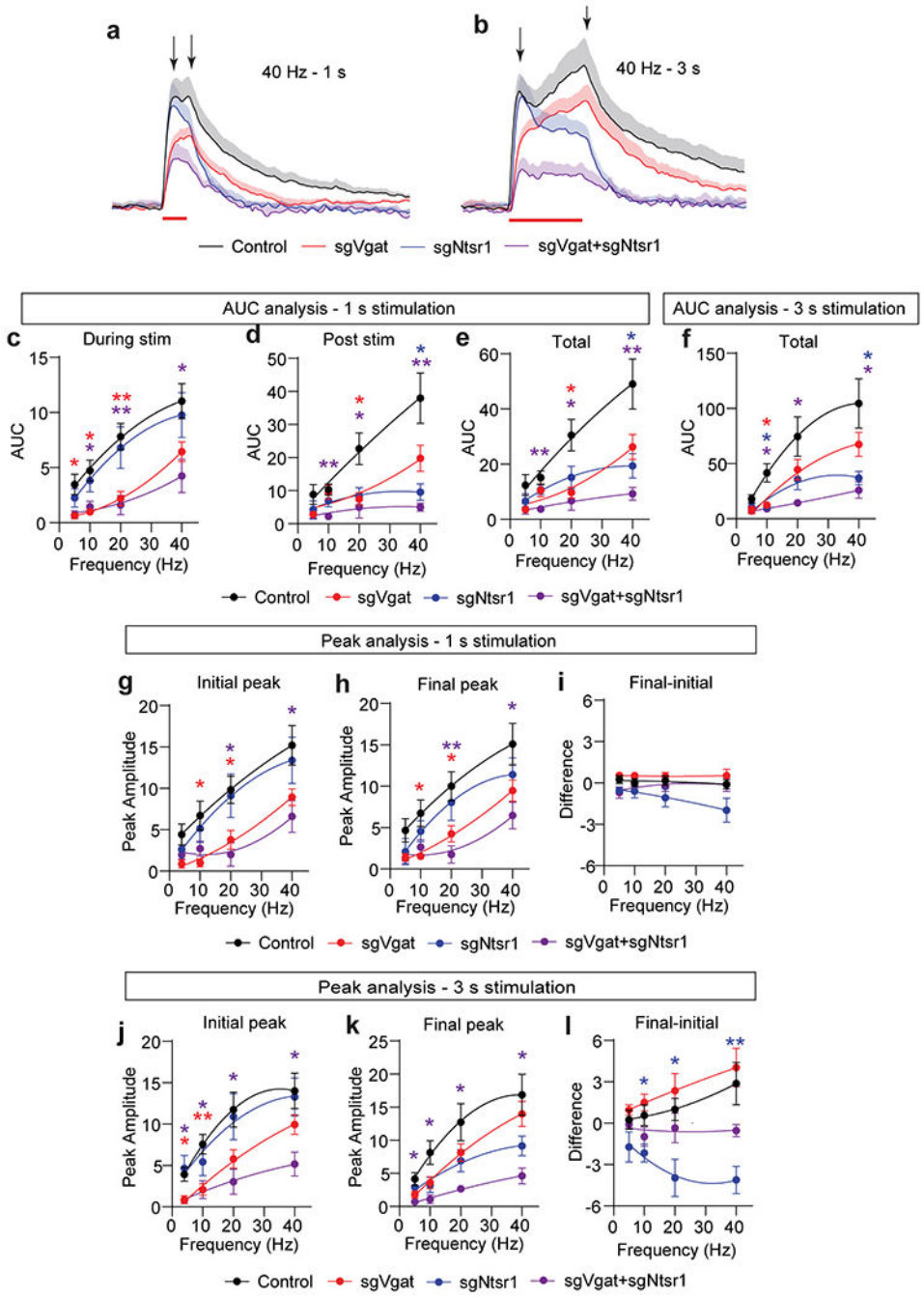

Extended Data Fig. 5. Analysis of evoked GCaMP6m signals in VTA-DA neurons.

(**a-b**) Average GCaMP6m fluorescence (Z-score) during and after 1 s (**a**) and 3 s (**b**) stimulation at 40 Hz. Arrows indicate initial and final peaks at the onset and offset of the stimulation, respectively. (**c**) Average area under the curve (AUC) of the Z-scored GCaMP6m fluorescence during 1 s stimulation at different frequencies. (**d**) Average AUC for the 10 s following 1 s stimulation at different frequencies. (**e**) Average AUC during and after 1 s stimulation at different frequencies. (**f**) Average AUC during and after 3 s stimulation at different frequencies. (**g**) Average initial peak amplitude (Z-score) of

GCaMP6m fluorescence during 1 s stimulation at different frequencies. (**h**) Average final peak amplitude (Z-score) of GCaMP6m fluorescence during 1 s stimulation at different frequencies. (**i**) Difference between final and initial peak amplitude (final-initial) of GCaMP6m fluorescence during 1 s stimulation at different frequencies. (**j**) Average initial peak amplitude (Z-score) of GCaMP6m fluorescence during 3 s stimulation at different frequencies. (**k**) Average final peak amplitude (Z-score) of GCaMP6m fluorescence during 3 s stimulation at different frequencies. (**l**) Difference between final and initial peak amplitude (final-initial) of GCaMP6m fluorescence during 3 s stimulation at different frequencies. (Control N=8, sgVgat N=,7 sgNtsr1 N=6, sgVgat+sgNtsr1 N=5. *P<0.05; **P<0.01; ***P<0.001; red asterisk sgVgat vs. control; blue asterisk sgNts vs. control; purple asterisk sgVgat+sgNtsr1 vs. control.) Data are presented as mean ± S.E.M.

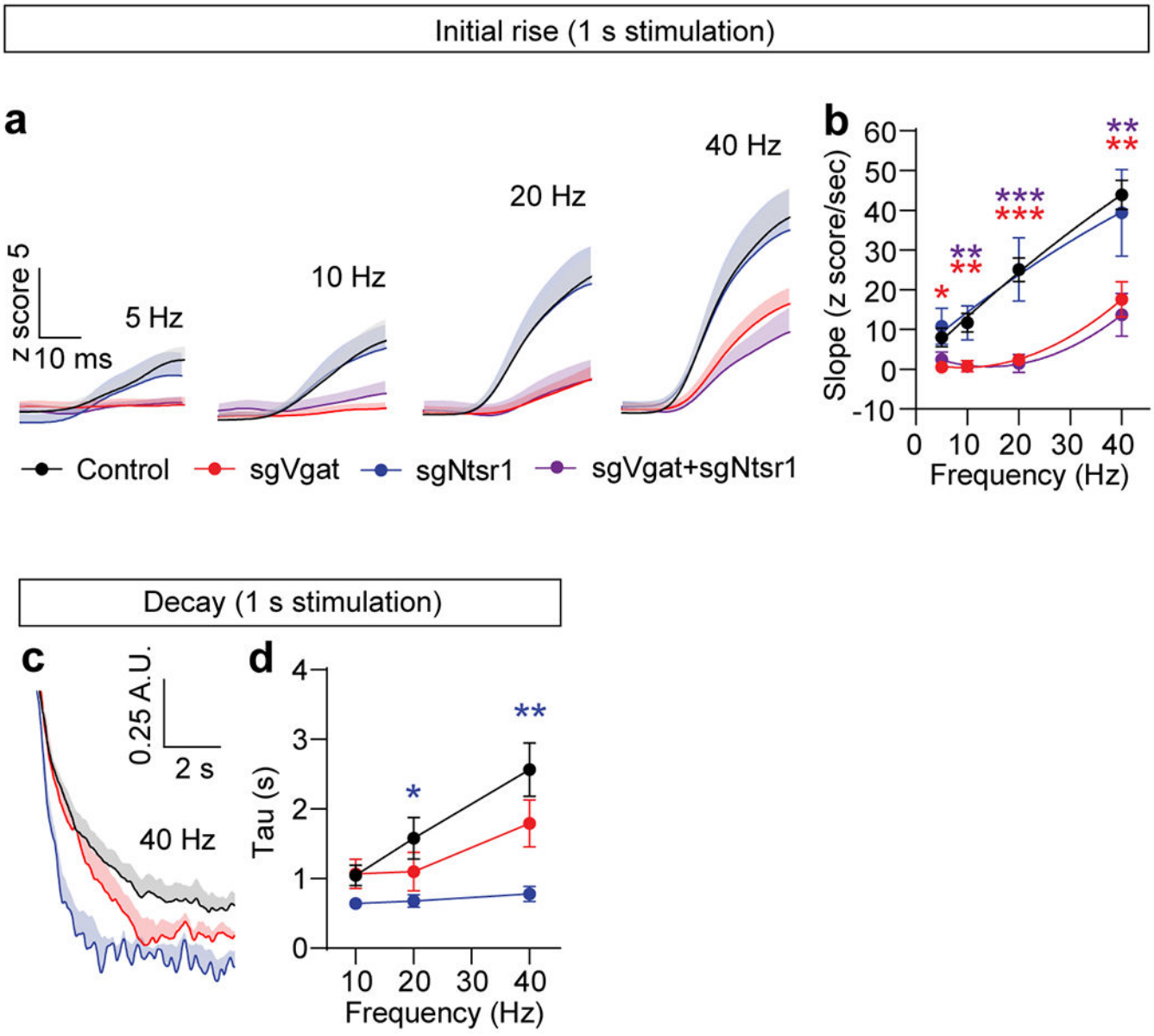

Extended Data Figure 6. Analysis of evoked GCaMP6m signals in VTA-DA neurons.

(a) Average GCaMP6m fluorescence during the onset of 1 s optical stimulation. (**b**) Average slope of the initial rise in GCaMP6m fluorescence at different stimulus frequencies with 1 s optical stimulation. (**c**) Average GCaMP6m fluorescence decay following termination of 1 s stimulation, normalized to peak. (**d**) Average decay time constant of GCaMP6m fluorescence at different stimulus frequencies for 1 s. Note: Analysis of 5 Hz was omitted due to lack of signal in sgVgat mice, and sgVgat+sgNtsr1 mice were excluded from analysis due to the low amplitude of the evoked fluorescence. (Control N=8, sgVgat N=,7 sgNtsr1 N=6, sgVgat+sgNtsr1 N=5. *P<0.05; **P<0.01; ***P<0.001; red asterisk sgVgat vs. control; blue asterisk sgNts vs. control; purple asterisk sgVgat+sgNtsr1 vs. control). Data are presented as mean ± S.E.M.

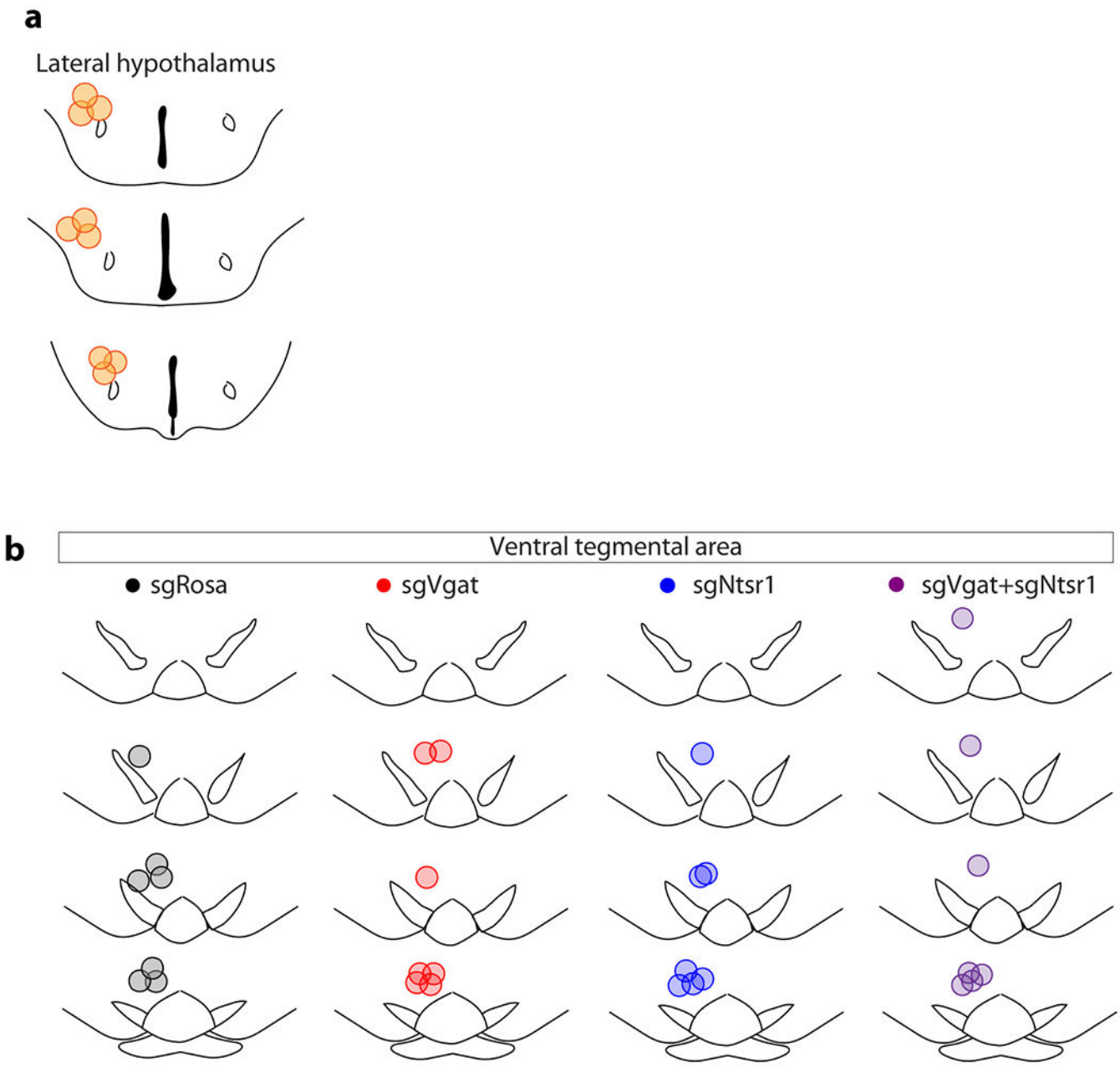

Extended Data Figure 7. Fiber placements for behavioral photometry experiments.
(a) Placements for recording fibers in LH. **(b**) Placements for recording fibers in VTA.

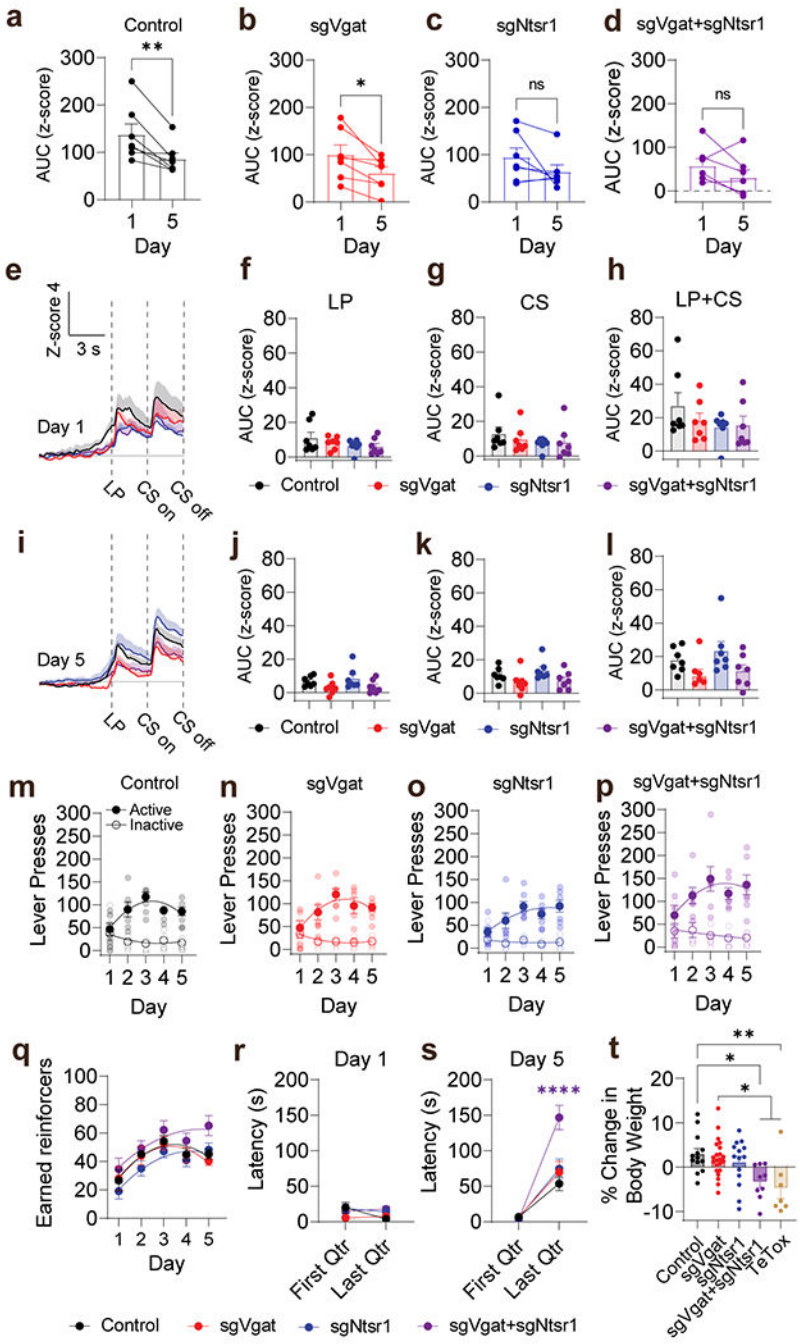

Extended Data Figure 8. Additional analysis of behavioral photometry data.

(a-d) AUC of the z-scored fluorescence for the 20 s following head entry on days 1 and 5 in the indicated groups (N=7 mice per group, *p<0.05, **P<0.01). **(e)** Average GCaMP6m fluorescence on day 1 aligned to rewarded lever presses. **(f)** AUC during the 3 s following the lever press on day 1. **(g)** AUC during the CS period on day 1. **(h)** AUC from 3 s prior to the lever press to the end of the CS period on day 1. **(i)** Average GCaMP6m fluorescence on day 5 aligned to rewarded lever presses. **(j)** AUC during the 3 s following the lever press on day 5. **(k)** AUC during the CS period on day 5. **(l)** AUC from 3 s prior to the lever press

to the end of the CS period on day 5. **(m-p)** Active and inactive lever presses across training days in the indicated groups. **(q)** Earned reinforcers across training days. **(r-s)** Latency to make a head entry into the food hopper following pellet delivery in the first or last quarter of the session on day 1 (r) or day 5 (s), averaged across all trials from all mice (****P<0.0001). **(t)** Percent change in body weight from pre-surgery weight to 5 weeks post viral injection (Control N=13 mice; sgVgat N=22 mice; sgNtsr1 N=14 mice; sgVgat+sgNtsr1 N=9 mice; TeTox N=7 mice; *p<0.05, **P<0.01). Data are presented as mean ± S.E.M.

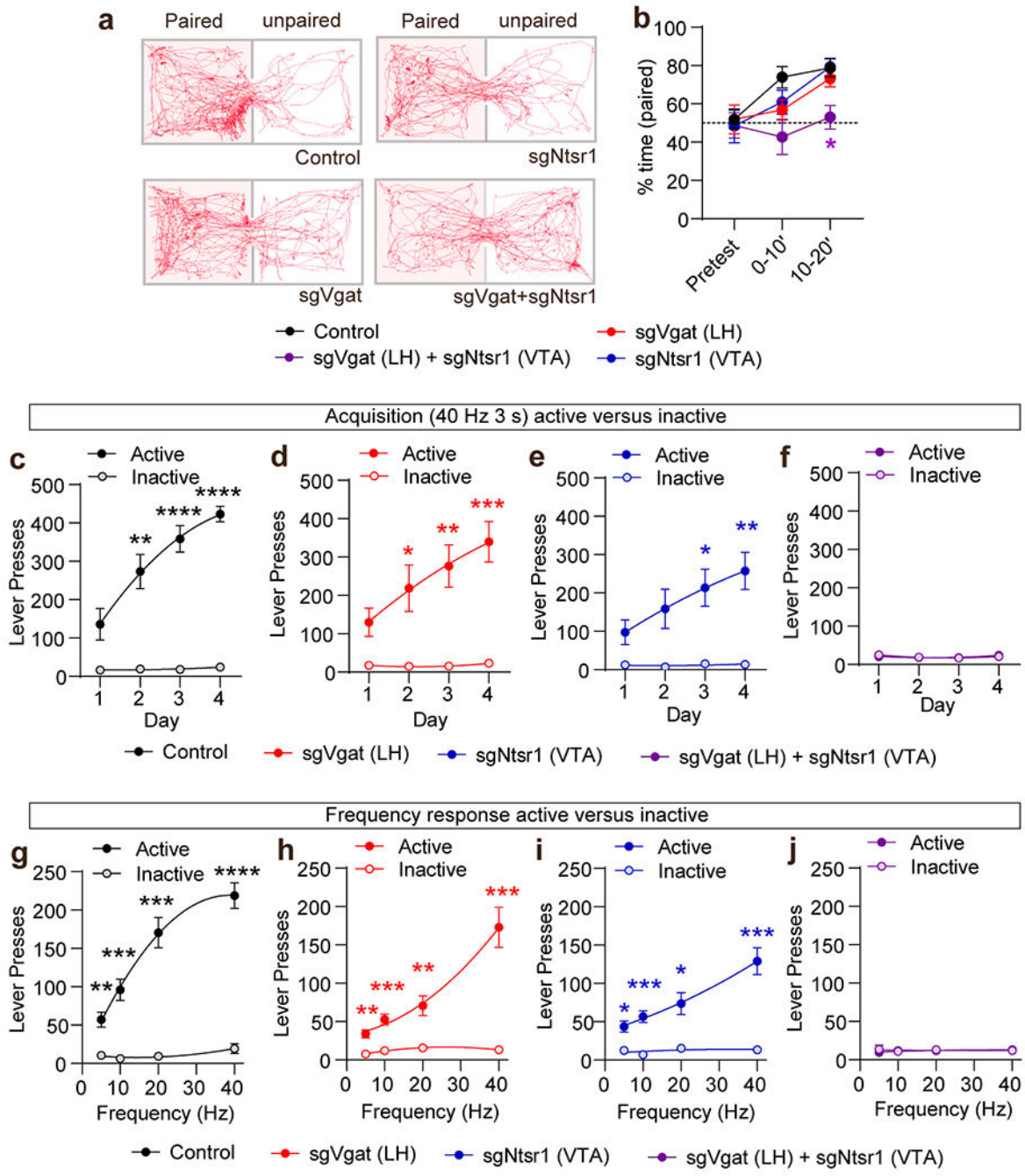

Extended Data Figure 9. Coordinated actions of LH-Nts GABA release and VTA-DA Ntsr1 in behavioral reinforcement.

(**a**) Representative behavioral tracks during RTPP. (**b**) Average percent time in the light-paired chamber during 10 min pretest, and the first and last 10 min of RTPP (*P<0.05; control N=8, sgVgat N=,10 sgNtsr1 N=9, sgVgat+sgNtsr1 N=10; purple asterisk sgVgat+sgNtsr1 vs. control). (**c-f**) Average active and inactive lever presses for the four groups of mice during acquisition. (**g-j**) Average active and inactive lever presses for the four groups of mice during frequency response analysis (**c-j:** control N=9, sgVgat N=10, sgNtsr1 N=8, sgVgat+sgNtsr1 N=10, *P<0.05; **P<0.01; ***P<0.001; ****P<0.0001). Data are presented as mean ± SEM.

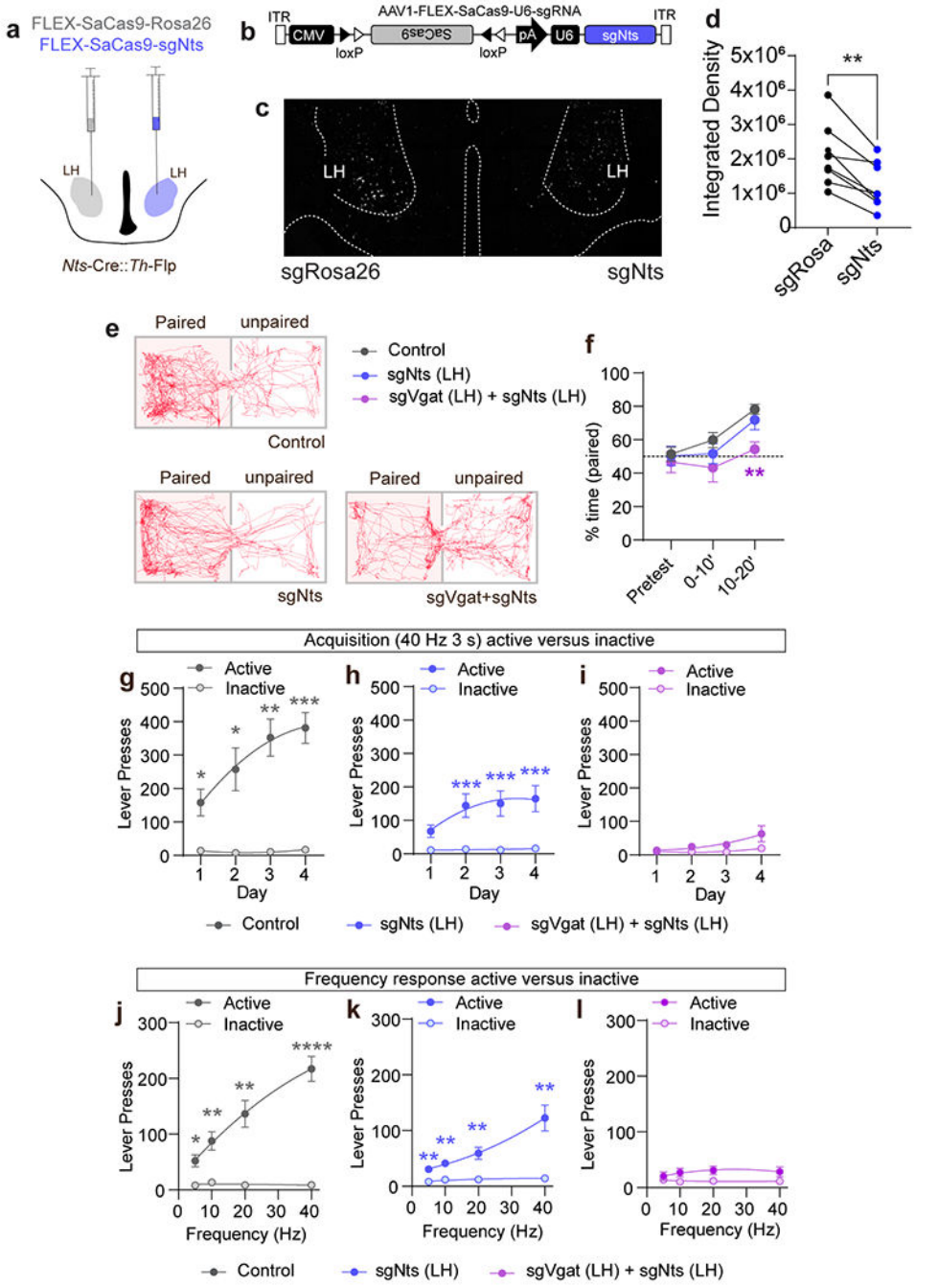

Extended Data Figure 10. Coordinated actions of LH-Nts GABA and Nts release in the VTA-DA for behavioral reinforcement.

(**a**) Schematic of unilateral injection of control virus (AAV1-FLEX-SaCas9-u6-sgRosa26 (grey)) and AAV1-FLEX-SaCas9-U6-sgNts (blue) into the LH of *Nts*-Cre mice. (**b**) Schematic of AAV1-FLEX-SaCas9-U6-sgNts viral vector. (**c**) Image of *in situ* hybridization for *Nts* in the sgRosa26 and sgNts injected sides of the LH. (**d**) Quantification of integrated pixel density of the fluorescent signal in the sgRosa26 and sgNts injected sides of the LH (**P<0.01; n=8 sections from N=4 mice). (**e**) Representative behavioral tracks during

RTPP from the four groups of mice. (**f**) Average percent time in the light-paired chamber during 10 min pretest, and the first and last 10 min of RTPP (**P<0.01; purple asterisk sgVgat+sgNts vs. control; control N=12; sgNts=10; sgNts+sgVgat N=8). (**g-i**) Average active versus inactive lever presses for the three groups of mice during acquisition. (**j-l**) Average active versus inactive lever presses for the three groups of mice during frequency response analysis (**g-l** ****P<0.0001; ***P<0.001; **P<0.01; *P<0.05; control N=9; sgNts N=11; sgVgat+sgNts N=7). Data are presented as mean ± SEM.

Supplementary Material

Refer to Web version on PubMed Central for supplementary material.

Acknowledgments:

Supported by National Institutes of Health grants R21 MH121774 (MES), R01 DA054924 (MES), and R01 DA044315 (LSZ). This work was also supported by the University of Washington Center of Excellence in Opioid Addiction Research (P30 DA048736). We thank Dr. James Allen, Dr. Avery Hunker, and Dasha Krayushkina for assistance with viral production, and Dr. Scott Ng-Evans for assistance with photometry analysis. We also thank members of the Zweifel lab for their thoughtful discussion.

Data availability:

All data associated with this study will be made available by the corresponding author upon reasonable request.

References

1. Bartfai T, Iverfeldt K, Fisone G & Serfozo P Regulation of the release of coexisting neurotransmitters. Annu Rev Pharmacol Toxicol 28, 285–310, doi:10.1146/annurev.pa.28.040188.001441 (1988). [PubMed: 2898236]
2. Hunker AC et al. Conditional Single Vector CRISPR/SaCas9 Viruses for Efficient Mutagenesis in the Adult Mouse Nervous System. Cell Rep 30, 4303–4316 e4306, doi:10.1016/j.celrep.2020.02.092 (2020). [PubMed: 32209486]
3. Salio C, Lossi L, Ferrini F & Merighi A Neuropeptides as synaptic transmitters. Cell Tissue Res 326, 583–598, doi:10.1007/s00441-006-0268-3 (2006). [PubMed: 16847638]
4. van den Pol AN Neuropeptide transmission in brain circuits. Neuron 76, 98–115, doi:10.1016/j.neuron.2012.09.014 (2012). [PubMed: 23040809]
5. Tritsch NX, Granger AJ & Sabatini BL Mechanisms and functions of GABA co-release. Nat Rev Neurosci 17, 139–145, doi:10.1038/nrn.2015.21 (2016). [PubMed: 26865019]
6. Nusbaum MP, Blitz DM & Marder E Functional consequences of neuropeptide and small-molecule co-transmission. Nat Rev Neurosci 18, 389–403, doi:10.1038/nrn.2017.56 (2017). [PubMed: 28592905]
7. Brown JA et al. Distinct Subsets of Lateral Hypothalamic Neurotensin Neurons are Activated by Leptin or Dehydration. Sci Rep 9, 1873, doi:10.1038/s41598-018-38143-9 (2019). [PubMed: 30755658]
8. Mickelsen LE et al. Single-cell transcriptomic analysis of the lateral hypothalamic area reveals molecularly distinct populations of inhibitory and excitatory neurons. Nat Neurosci 22, 642–656, doi:10.1038/s41593-019-0349-8 (2019). [PubMed: 30858605]
9. Soden ME et al. Anatomic resolution of neurotransmitter-specific projections to the VTA reveals diversity of GABAergic inputs. Nat Neurosci 23, 968–980, doi:10.1038/s41593-020-0657-z (2020). [PubMed: 32541962]

10. Wise RA Dopamine, learning and motivation. Nat Rev Neurosci 5, 483–494, doi:10.1038/nrn1406 (2004). [PubMed: 15152198]
11. Olds J & Milner P Positive reinforcement produced by electrical stimulation of septal area and other regions of rat brain. J Comp Physiol Psychol 47, 419–427, doi:10.1037/h0058775 (1954). [PubMed: 13233369]
12. Olds J, Travis RP & Schwing RC Topographic organization of hypothalamic self-stimulation functions. J Comp Physiol Psychol 53, 23–32, doi:10.1037/h0039776 (1960). [PubMed: 14428621]
13. Jennings JH et al. Visualizing hypothalamic network dynamics for appetitive and consummatory behaviors. Cell 160, 516–527, doi:10.1016/j.cell.2014.12.026 (2015). [PubMed: 25635459]
14. Kempadoo KA et al. Hypothalamic neurotensin projections promote reward by enhancing glutamate transmission in the VTA. J Neurosci 33, 7618–7626, doi:10.1523/JNEUROSCI.2588-12.2013 (2013). [PubMed: 23637156]
15. Nieh EH et al. Inhibitory Input from the Lateral Hypothalamus to the Ventral Tegmental Area Disinhibits Dopamine Neurons and Promotes Behavioral Activation. Neuron 90, 1286–1298, doi:10.1016/j.neuron.2016.04.035 (2016). [PubMed: 27238864]
16. Patterson CM et al. Ventral tegmental area neurotensin signaling links the lateral hypothalamus to locomotor activity and striatal dopamine efflux in male mice. Endocrinology 156, 1692–1700, doi:10.1210/en.2014-1986 (2015). [PubMed: 25734363]
17. Boyden ES, Zhang F, Bamberg E, Nagel G & Deisseroth K Millisecond-timescale, genetically targeted optical control of neural activity. Nature neuroscience 8, 1263–1268, doi:10.1038/nn1525 (2005). [PubMed: 16116447]
18. Szigethy E & Beaudet A Correspondence between high affinity 125I-neurotensin binding sites and dopaminergic neurons in the rat substantia nigra and ventral tegmental area: a combined radioautographic and immunohistochemical light microscopic study. J Comp Neurol 279, 128–137, doi:10.1002/cne.902790111 (1989). [PubMed: 2563267]
19. Opland D et al. Loss of neurotensin receptor-1 disrupts the control of the mesolimbic dopamine system by leptin and promotes hedonic feeding and obesity. Mol Metab 2, 423–434, doi:10.1016/j.molmet.2013.07.008 (2013). [PubMed: 24327958]
20. Woodworth HL, Perez-Bonilla PA, Beekly BG, Lewis TJ & Leinninger GM Identification of Neurotensin Receptor Expressing Cells in the Ventral Tegmental Area across the Lifespan. eNeuro 5, doi:10.1523/ENEURO.0191-17.2018 (2018).
21. Jiang ZG, Pessia M & North RA Neurotensin excitation of rat ventral tegmental neurones. J Physiol 474, 119–129, doi:10.1113/jphysiol.1994.sp020007 (1994). [PubMed: 8014889]
22. Catterall WA Voltage-gated calcium channels. Cold Spring Harb Perspect Biol 3, a003947, doi:10.1101/cshperspect.a003947 (2011). [PubMed: 21746798]
23. Snider RM, Forray C, Pfenning M & Richelson E Neurotensin stimulates inositol phospholipid metabolism and calcium mobilization in murine neuroblastoma clone N1E-115. J Neurochem 47, 1214–1218, doi:10.1111/j.1471-4159.1986.tb00742.x (1986). [PubMed: 3018165]
24. Chen TW et al. Ultrasensitive fluorescent proteins for imaging neuronal activity. Nature 499, 295–300, doi:10.1038/nature12354 (2013). [PubMed: 23868258]
25. Klapoetke NC et al. Independent optical excitation of distinct neural populations. Nature methods 11, 338–346, doi:10.1038/nmeth.2836 (2014). [PubMed: 24509633]
26. Ramirez-Virella J & Leinninger GM The Role of Central Neurotensin in Regulating Feeding and Body Weight. Endocrinology 162, doi:10.1210/endocr/bqab038 (2021).
27. Schultz W, Dayan P & Montague PR A neural substrate of prediction and reward. Science 275, 1593–1599, doi:10.1126/science.275.5306.1593 (1997). [PubMed: 9054347]
28. Soden ME et al. Distinct Encoding of Reward and Aversion by Peptidergic BNST Inputs to the VTA. Front Neural Circuits 16, 918839, doi:10.3389/fncir.2022.918839 (2022). [PubMed: 35860212]
29. Chung AS, Miller SM, Sun Y, Xu X & Zweifel LS Sexual congruency in the connectome and translatome of VTA dopamine neurons. Sci Rep 7, 11120, doi:10.1038/s41598-017-11478-5 (2017). [PubMed: 28894175]

Methods References

30. Poulin JF et al. Mapping projections of molecularly defined dopamine neuron subtypes using intersectional genetic approaches. Nat Neurosci 21, 1260–1271, doi:10.1038/s41593-018-0203-4 (2018). [PubMed: 30104732]

31. Gore BB, Soden ME & Zweifel LS Manipulating gene expression in projection-specific neuronal populations using combinatorial viral approaches. Curr Protoc Neurosci 65, 4 35 31–20, doi:10.1002/0471142301.ns0435s65 (2013).

32. Ting JT, Daigle TL, Chen Q & Feng G Acute brain slice methods for adult and aging animals: application of targeted patch clamp analysis and optogenetics. Methods Mol Biol 1183, 221–242, doi:10.1007/978-1-4939-1096-0_14 (2014). [PubMed: 25023312]

33. Hunker AC & Zweifel LS Protocol to Design, Clone, and Validate sgRNAs for In Vivo Reverse Genetic Studies. STAR Protoc 1, doi:10.1016/j.xpro.2020.100070 (2020).

34. Brinkman EK, Chen T, Amendola M & van Steensel B Easy quantitative assessment of genome editing by sequence trace decomposition. Nucleic Acids Res 42, e168, doi:10.1093/nar/gku936 (2014). [PubMed: 25300484]

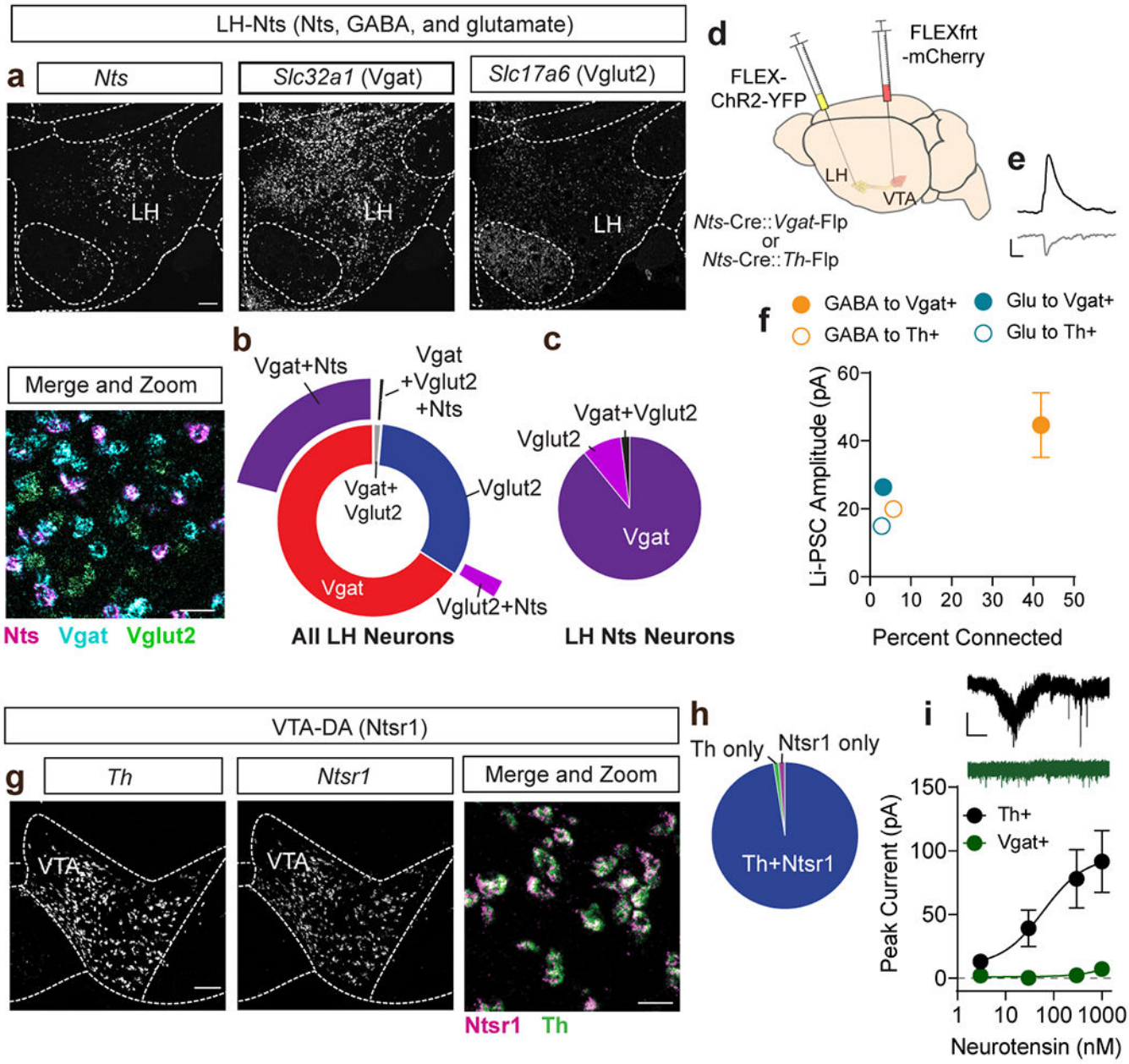

Figure 1. Connectivity of LH-Nts neurons and Ntsr1 signaling in the VTA.

(**a**) *In situ* hybridization in the LH for *Nts, Slc32a1* (Vgat), and *Slc17a6* (Vglut2). Scale bars = 150 μm (greyscale images) and 25 μm (zoom). (**b**) Quantification of all Nts, Vgat, and Vglut2 expressing neurons in the LH. (**c**) Quantification of Vgat and Vglut2 expressing Nts neurons of the LH. (**d**) Schematic of viral injection strategy for slice electrophysiology. (**e**) Example traces of inhibitory (top) and excitatory (bottom) light-evoked postsynaptic currents (Li-PSCs) onto VTA neurons (scale bar = 25 pA, 10 ms). (**f**) Percent of recorded neurons with a detectable Li-PSC and average Li-PSC amplitude recorded from VTA Vgat+ or Th+ neurons (GABA to Vgat n=13/31 cells, GABA to Th n=2/35 cells, Glu to Vgat n=1/31 cells, Glu to Th n=1/35 cells). (**g**) *In situ* hybridization in the VTA for *Th* and

Ntsr1. Scale bars = 150 μm (greyscale images) and 25 μm (zoom). (**h**) Quantification of *Th* and *Ntsr1* expressing neurons of the VTA. (**i**) Example traces and quantification of currents evoked by bath NTS in VTA-DA (black) and VTA-GABA neurons (green); (scale bar=50 pA, 20 s, n=4-10 cells/data point from N=2-3 mice). **b,c and h**, see Supplementary Table 1 for cell counts. Data are presented as mean ± standard error of the mean (SEM).

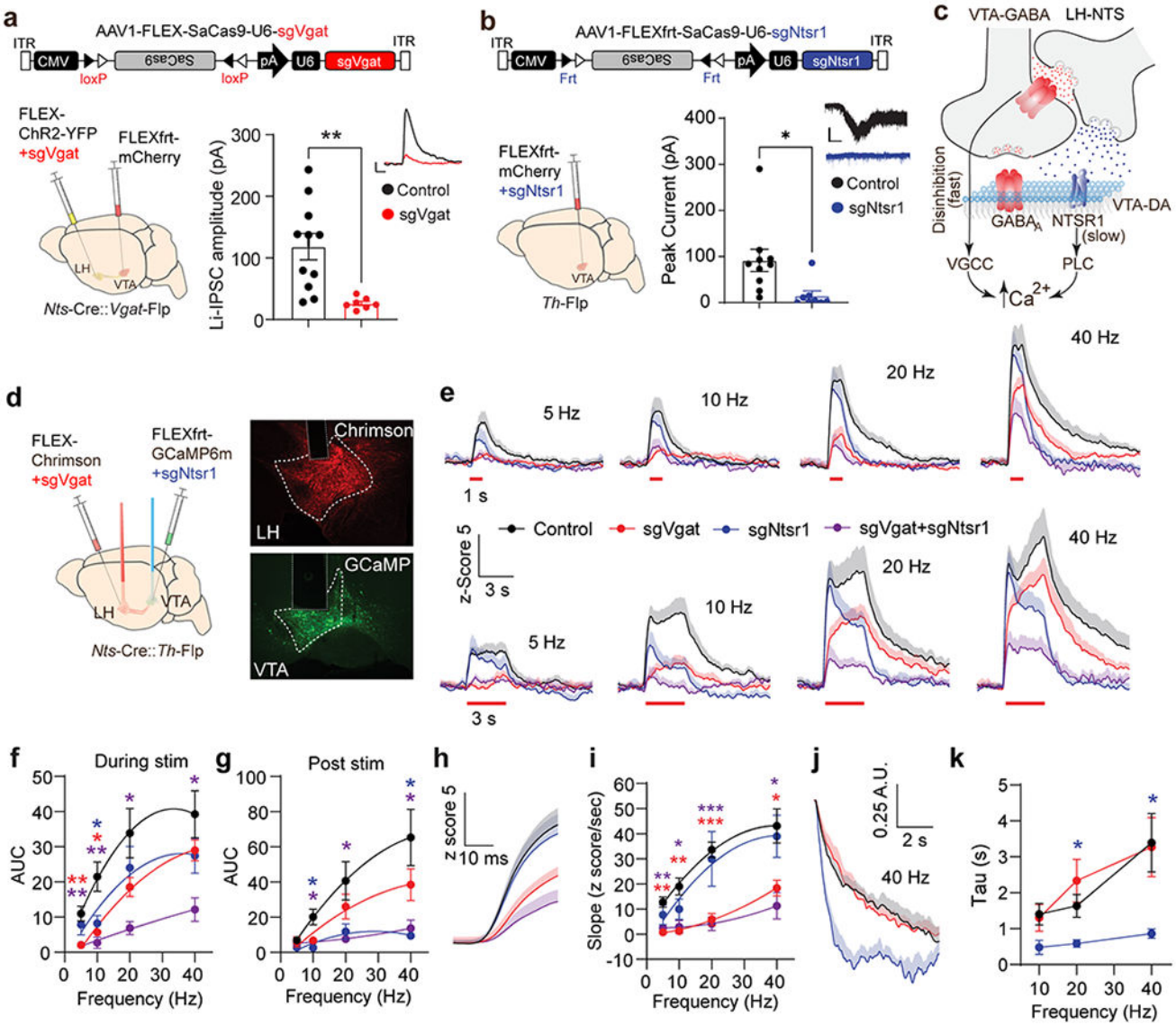

Figure 2. LH-Nts evoked calcium signals in the VTA are regulated by GABA release and Ntsr1 signaling.

(**a-b**) Schematics for Cre-dependent CRISPR targeting (top) and viral injections (bottom left). (**a**) Quantification and example traces of Li-IPSCs recorded in VTA-GABA neurons with control CRISPR or sgVgat expression in LH-NTS neurons (bottom right; control, n=11 cells from N=3 mice; sgVgat n=7 cells from N=3 mice; **P<0.01, scale bar: 25 pA, 10 ms). (**b**) Quantification and example traces of currents evoked by 1 μM bath NTS (bottom right; control, n=10 cells from N=3 mice; sgNtsr1 n=8 cells from N=2 mice; *P<0.05, scale bar: 20 s, 50 pA). (**c**) Proposed model of calcium signals in VTA-DA neurons. (**d**) Schematic of viral injection and fiber implantation (left) and expression of Chrimson-tdTomato and GCaMP6m in the LH and VTA with representative optical fiber placements for stimulation and imaging (right). (**e**) Average GCaMP6m fluorescence (Z-score) following 1 s (top) or 3 s (bottom) stimulation at different frequencies. (**f-g**) Average area under the curve (AUC) of the Z-scored GCaMP6m fluorescence during (**f**) and for

10 s following (**g**) stimulation at different frequencies (3 s stim). (**h)** Average GCaMP6m fluorescence (Z-score) at the onset of 3 s, 40 Hz optical stimulation. **(i)** Average slope of the initial rise in GCaMP6m fluorescence at different stimulus frequencies (3 s stim). **(j)** Average GCaMP6m fluorescence decay following termination of 3 s stimulation, normalized to peak. (**k**) Average decay time constant (tau) of GCaMP6m fluorescence at different stimulus frequencies for 3 s stimulation. (**e-k**, control N=8, sgVgat N=7, sgNtsr1 N=6, sgVgat+sgNtsr1 N=5; Post-hoc comparisons: *P<0.05, **P<0.01, ***P<0.001, red asterisk sgVgat vs. control; blue asterisk sgNtsr1 vs. control; purple asterisk sgVgat+sgNtsr1 vs. control.) See Supplementary Table 2 for details on statistical tests. Data are presented as mean ± SEM.

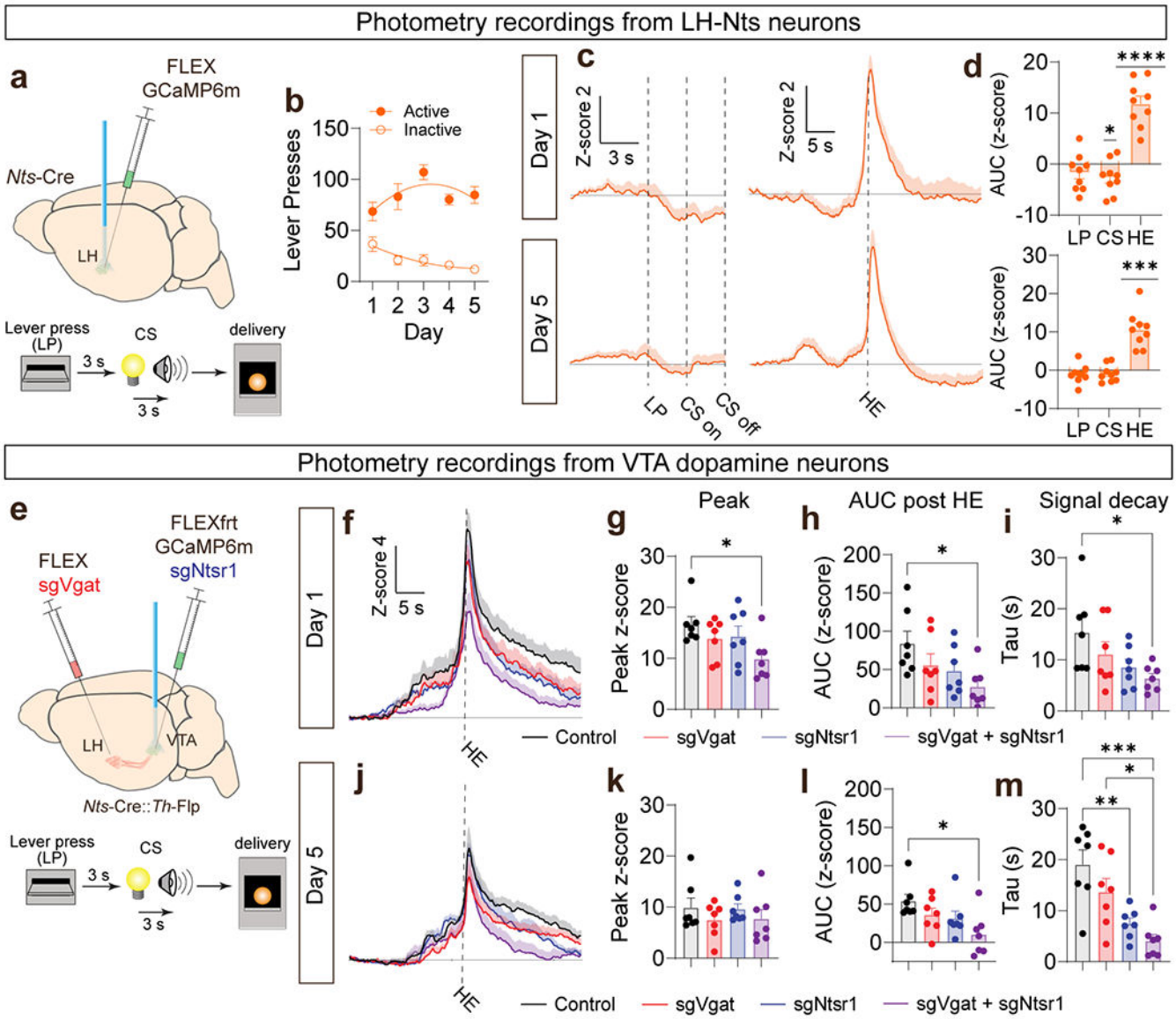

Figure 3. LH-Nts neurons contribute to activation of VTA-DA neurons during reward retrieval.

(a) Schematic of viral injection and fiber implantation to record from LH-Nts neurons (top), schematic of operant paradigm (bottom). **(b)** Active and inactive lever presses across 5 days of training. **(c)** Average GCaMP6m fluorescence (Z-score) in LH-Nts neurons on day 1 (top) or day 5 (bottom) of operant conditioning. Left: response to lever press (LP) and cue (CS) presentation. Right: response to first head entry (HE) into the food hopper following reward delivery. **(d)** AUC for the 3 s following the LP, the 3 s during the cue delivery, or the 3 s following HE (N=9 mice, 1-sample t-test to determine significant difference from zero: *P<0.05, ***P<0.001, ****P<0.0001). **(e)** Schematic of viral injection and fiber implantation to record from VTA-DA neurons (top), schematic of operant paradigm (bottom). **(f)** Average GCaMP6m fluorescence (Z-score) on day 1 of conditioning, aligned to first HE following reward delivery. **(g)** Peak Z-score, **(h)** AUC from 5 to 20 s following HE, and **(i)** Decay time constant (Tau) following HE on day 1 of conditioning. **(j)** Average

GCaMP6m fluorescence (Z-score) on day 5 of conditioning, aligned to first HE. **(k)** Peak Z-score, **(l)** AUC from 5 to 20 s following HE, and **(m)** Decay time constant (Tau) following HE, on day 5 of conditioning. (**f-m**: N=7 mice per group. *P<0.05, **P<0.01, ***P<0.001 for indicated post-hoc comparisons. For panel **g** ANOVA P = 0.0552, post-hoc P = 0.0205.) See Supplementary Table 2 for details on statistical tests. Data are presented as mean ± SEM.

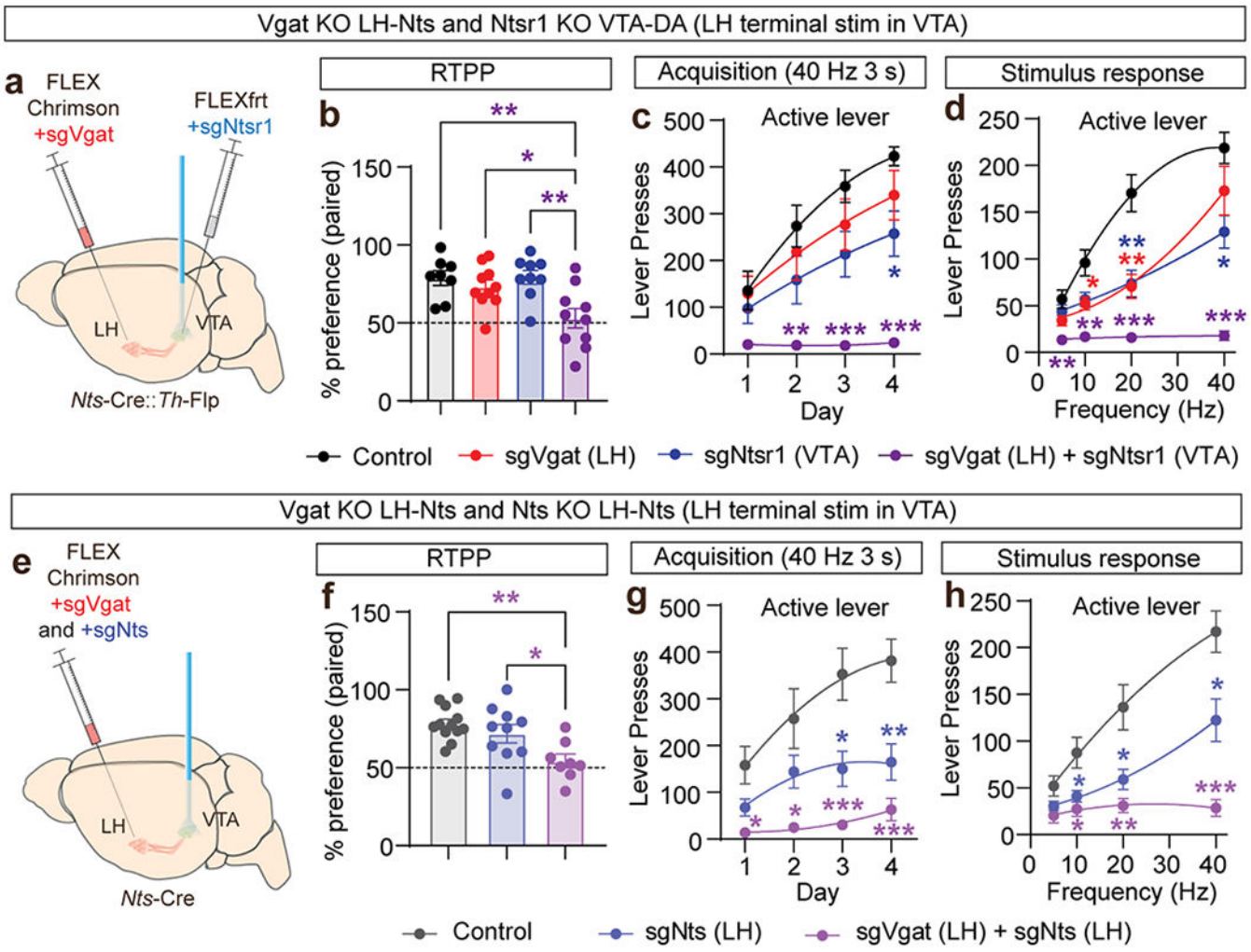

Figure 4. Coordinated actions of LH-Nts and GABA co-release in behavioral reinforcement.

(**a**) Schematic of viral injections and stimulating fiber placement. **(b)** Average percent time in light-paired (20 Hz) chamber during final 10 min of RTPP (**P<0.01; *P<0.05; control N=8, sgVgat N=,10 sgNtsr1 N=9, sgVgat+sgNtsr1 N=10). (**c**) Average active lever press responses (60 min session) for 40 Hz, 3 s optical stimulation of LH-Nts inputs to the VTA. (**d**) Average active lever presses (30 min session) for optical stimulation of LH-Nts inputs to the VTA at different frequencies (**c,d** ***P<0.001; **P<0.01; *P<0.05; red asterisk sgVgat vs. control; blue asterisk sgNtsr1 vs. control; purple asterisk sgVgat+sgNtsr1 vs. control; control N=9, sgVgat N=,10 sgNtsr1 N=8, sgVgat+sgNtsr1 N=10). (**e**) Schematic of viral injections and stimulating fiber placement. (**f**) Average percent time in light-paired (20 Hz) chamber during final 10 min of RTPP (**P<0.01; *P<0.05; control N=12; sgNts=10; sgNts+sgVgat N=8). (**g**) Average active lever press responses (60 min session) for 40 Hz, 3 s optical stimulation of LH-Nts inputs to the VTA. (**h**) Average active lever presses (30 min session) for optical stimulation of LH-Nts inputs to the VTA at different frequencies (**g,h** ***P<0.001; **P<0.01; *P<0.05; blue asterisk sgNtsr1 vs. control; purple

asterisk sgVgat+sgNtsr1 vs. control; control N=9; sgNts N=11; sgVgat+sgNts N=7). See Supplementary Table 2 for details on statistical tests. Data are presented as mean ± SEM.